UNIVERSITY OF CALIFORNIA,

IRVINE

Mathematical Modeling of Polymer Electrolyte Membrane Water Electrolysis Cell with a Component-level Approach

THESIS

submitted in partial satisfaction of the requirements

for the degree of

MASTER OF SCIENCES

In Mechanical and Aerospace Engineering

by

Daniela Fernanda Ruiz Diaz

Thesis Committee:

Professor Yun Wang, Chair

Professor Manuel Gamero Castaño

Assistant Professor Edwin Peraza Hernandez

2021

DEDICATION

I dedicate this thesis to my family and many friends, with special gratitude to my loving parents, Karla Díaz, and Matias Ruiz whose words of encouragement have helped me with all my preparation. My sisters Montserrat and Cristina Ruiz, and my best friend Margarita Rivera that have never left my side and have encouraged me through the journey.

No te rindas que la vida es eso,
Continuar el viaje,
Perseguir tus sueños,
Destrabar el tiempo,
Correr los escombros,
Y destapar el cielo.

(Mario Benedetti
No te rindas)

TABLE OF CONTENTS

Page

LIST OF FIGURES

Page

`

LIST OF TABLES

ACKNOWLEDGEMENTS

I would like to thank my committee chair Professor Yun Wang, for his advice, support, and patience during the process. His experience and constant help have encouraged me in this journey of my academic research and daily life. I would also like to thank Professor Manuel Gamero Castaño and Professor Edwin Peraza Hernandez for their support on my thesis. I would like to thank the Consejo Nacional de Ciencia y Tecnología (CONACYT) in Mexico for their financial support.

ABSTRACT OF THE THESIS

Mathematical Modeling of Polymer Electrolyte Membrane Water Electrolysis Cell with a Component-level Approach

by

Daniela Fernanda Ruiz Diaz

Master of Sciences in Mechanical and Aerospace Engineering

University of California, Irvine, 2021

Professor Yun Wang, Chair

Nowadays, Proton Exchange Membrane Electrolysis Cells (PEMEC) have gained interest for being one of the most promising technologies for high-purity hydrogen production with zero emissions when coupled with renewable energy. Therefore, studying the factors affecting PEMEC performance is one of the most important areas of study for this technology. This work presents a component-level PEMEC model describing water exchange between electrodes, proton conductance, electrochemical reaction kinetics, two-phase oxygen-liquid water mixture in the flow channel, and two-phase transport in the porous transport layer (PTL). At the channel/PTL interface, an interfacial resistance sub-model is proposed for oxygen removal. The model investigates the cell performance under high current density considering 1.) homogeneous properties in each component, 2.) isothermal conditions, and 3.) Tafel equation to approximate electrochemical reaction kinetics. The model is implemented in MATLAB/Simulink for predicting the contribution of the different voltage losses to the polarization curve under different temperature (40℃ to 80℃), pressure (1 to 10 bar), current density (0 to 5A/cm^2), and liquid saturation percentages (100% to 45%). The present model is validated against various sets of experimental data available in the literature. The obtained results show that ohmic and activation

overpotential contribute to a major voltage loss representing about 27% and 19% when working at 5A/cm^2, 1 atm, and 80℃. Additionally, when working at high current density, oxygen bubbles are found to occupy an areal portion as large as 55% at the PTL/Ch interface, blocking the available region for water transport to the catalyst layer and reducing the cell performance. Furthermore, high-temperature operation helps the overall voltage by decreasing it around 4% from 40℃ to 60℃ and about 8% from 60℃ to 80℃. Increase in operating pressure raises the overall voltage of the cell. However, the voltage rise is considered small compared to the effects of temperature. PEMEC modeling is a powerful tool for predicting hydrogen generation. This is especially true when considering a two-phase oxygen-liquid water mixture flow and two-phase transport while working under high current densities, which is considered the most important contribution of this work.

Chapter 1. Literature review

According to the 2019 Global Energy Statistical Yearbook, the US was ranked second place in energy consumption of about 2,258 Mtoe in 2019 following China with 3,284 Mtoe in 2019 [83], and due to growing concerns of fossil fuel depletion and climate change, researchers have been seeking alternatives for sustainable energy generation. As a result, hydrogen has drawn a lot of attention as it can be used as a continuous generation source and it is an environmentally friendly alternative. Nowadays, there are many technologies available for hydrogen production that seem to be a promising alternative for this problem. Within these technologies are solid oxide water electrolysis (SOEC), alkaline water electrolysis (AWEC), and proton exchange membrane water electrolysis (PEMWEC). PEM water electrolysis offers several advantages like working under high current densities, and pressure, reaching higher efficiencies around 80-90% [20]. However, due to these operation conditions, several problems reach attention such as mass transport losses, ohmic, and activation overpotentials that reduce the performance of the cell.

1.1. Introduction to water electrolysis and electrolysis cells

Hydrogen demand is constantly growing, and it is expected to reach a global demand higher than 500 Mt/year by 2070, eight times more than 2019 [105]. Most of the global hydrogen current demand is produced from natural gas by steam reforming. During the process, carbon dioxide is emitted, making this method a non-sustainable one [106], helping researchers to make valuable strides for hydrogen production. Water is the most reliable source of hydrogen since it is sustainable due to its ease of being combined with renewables. The excess energy generated by a renewable system can be used to generate hydrogen by means of water electrolysis.

In 1800, William Nicholson and Anthony Carlisle reported to used Alessandro Volta's invention about the voltaic pile to split water, identifying hydrogen and oxygen as the produced species and establishing the concept of water electrolysis [69,107]. The physics behind electrolysis were explained thirty-three years later by Michael Faraday, who was able to establish a mathematical relationship between the mass of the species involved and the amount of electricity passing through the cell [8]. The mathematical equations related to water splitting reaction are explained later in this chapter.

Water splitting has many advantages since it is a mature technology that provides high purity hydrogen with one of the simplest approaches with zero emissions and high efficiency. Despite these, several aspects remain under study to optimize the efficiency of the cell and achieve a lower cost of the produced hydrogen and the cell itself to make this technology competitive as conventional ones.

1.2.Hydrogen production

Hydrogen is the lightest element in the periodic table and the most abundant chemical substance in the Universe, being the 10^{th} most abundant element on planet Hearth [77] and has a high gravimetric energy density of ~120kJ/kg [48], but as mentioned before it needs to be produce since in nature, it is found as a part of another substance such as alcohol, hydrocarbons, biomass, and water [62].

Two of the most widely used methods for Hydrogen production are Steam Methane Reforming (SMR) from fossil energy and water electrolysis. SMR separates the hydrogen from the carbon atoms in methane, and the process is done in two stages, first, the natural gas is mixed with steam and reacts in the presence of a catalyst [3,62] producing not only the desirable output

(H_2), but also carbon monoxide. In the second stage (Water-gas shift reaction), Carbon monoxide and steam react in the presence of a catalyst producing carbon dioxide and more hydrogen [75], hence this process contributes to the Greenhouse gas emissions.

Water electrolysis, on the other hand, represents a low polluting way to produce high purity hydrogen, and the energy required for the process can be supplied from renewable sources [41], thus hydrogen becomes as green as the source. According to the International Energy Agency, in 2019, the low-carbon hydrogen production was about 0.36 Mt/year and it is expected to increase to 7.97 Mt/ year by 2030 [30] thanks to the demand of the industry, followed by the transport sector and power production [31].

1.3. Water electrolysis

Water electrolysis is the process where electricity is applied to split water into hydrogen and oxygen. The electrolysis cell or electrolyzer is where the process takes place; it consists of two electrodes (Anode and Cathode) that are separated by a membrane and an electrolyte (ion conductor). The electrodes are connected through an external circuit. When a current is applied, electrons flow to the cathode (negative electrode) and are removed from water at the anode (positive electrode). Hydrogen ions travel from the anode to the cathode, where they get recombined to produce hydrogen (reduction reaction), and oxygen is formed at the anode (oxidation reaction). The energetic efficiency of electrolysis goes from around 50-70% [33].

Although electrolysis of water is a process that is well established today, there are still several issues that require attention to increase hydrogen conversion efficiency and lower the cost of production. An aspect that is of great interest for research is the two-phase flow phenomena that occurs in the electrolysis of water. When the separation process takes place, part

of the oxygen produced is in the form of bubbles and another part is dissolved. Oxygen bubbles are a concern as they can obstruct the space available for the water to react, causing the efficiency and therefore also the hydrogen production to decrease.

1.3.1. Fuel cells

Similarly, Fuel Cells (FC) is an entrenched technology where hydrogen and oxygen get recombined through an electrochemical conversion to produce current, heat, and water as the only reaction product [98]. A FC consists of two electrodes (anode and cathode) that are electron conductive, an electrolyte that should be proton conductive and electrical insulator, a separator, and an external circuit [100]. The most common type of FC is the Proton Exchange Membrane (PEMFC) that can also work as an electrolyzer. When the cell is operated in fuel cell mode, hydrogen fuel is supplied to the anode and gets oxidized to produce protons and electrons, protons migrate to the cathode through the electrolyte and electrons through the external circuit to get recombined with oxygen to form water [101].

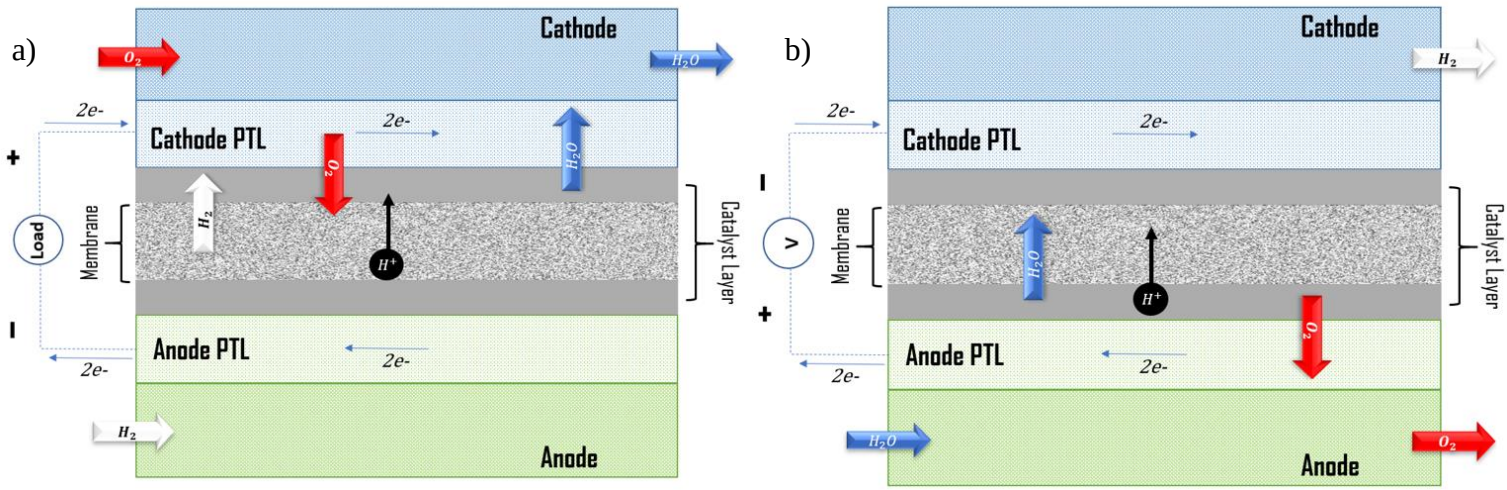

Figure 1. Basic schematic of a) PEM Fuel Cells (PEMFC) and b) PEM Electrolysis Cells (PEMECs).

When working in PEMEC mode, the process is reversed (including the current) [97] as indicated in Figure 1. Many fundamentals in PEM fuel cells are applicable to PEMECs, such as two-phase flow, electrochemical kinetics, and even materials. Numerous modeling studies are available in the literature regarding PEMFCs, and most PEMEC models have been adapted from these, hence, more modeling work needs to be developed regarding PEMECs.

1.4. Water electrolysis fundamentals

As previously mentioned, electrolysis of water is the process where water is decomposed using electricity to produce oxygen and high purity hydrogen (~99.999 vol%) that can be directly used in fuel cells, a combination that is expected to provide better diffusion of electricity to the grid and storage energy system [20,108]. It is considered the most important hydrogen production method since no fossil fuels are required for the process, it is considered to be simple, and no pollutant emissions are present [89].

The research in the area has been focused on finding ways to reduce the energy consumption required for hydrogen production, one of the main concerns related to hydrogen production by means of water electrolysis. To achieve a lower electricity need, it is important to understand the fundamentals of water electrolysis that are related to the electrocatalysts used for a series of electrochemical reactions that make water splitting possible. In this section, the fundamentals of water electrolysis will be introduced.

1.4.1. Typical structure of water electrolyzers

As mentioned before, the reaction of interest is the separation of water into hydrogen and oxygen. This reaction is possible by means of electric energy being converted into chemical energy. The typical components of an electrolytic cell consist of an external power supply,

electrolyte (water), a membrane, and two electrodes (anode and cathode) [89]. Electrodes are usually coated with a catalyst layer to accelerate the desired reaction. Since hydrogen and oxygen are the desired byproducts, the membrane (usually made by a porous material) acts like a separator to facilitate the accumulation of these two species and prevent them mixing again since hydrogen and oxygen by nature tend to easily mix, making the membrane one of the most important parts of the cell. The type of membrane utilized is used to classify the type of water electrolysis technology.

1.4.2. Types of water electrolyzers

Hydrogen technologies are a key tool to the zero-carbon emissions development that science is looking. Water electrolyzers are classified according to the type of electrolyte used, along with other characteristics such as operating conditions and their reachable efficiencies. The electrolyte (usually a membrane or diaphragm) serves as a separator for the two half-reactions (oxygen and hydrogen evolution reactions) taking place at each side of the cell (anode and cathode) [6,8,20].

The main types of electrolysis technologies can be classified as Alkaline water electrolysis (AWE), Solid Oxide water electrolysis (SOWE), and Polymer Electrolyte Membrane water electrolysis (PEMWE) [36,64]. AWE most commonly use a potassium hydroxide solution as electrolyte due to its high conductivity [109], SOWE utilize a ceramic material to transport ions from oxygen since they work under high-temperature conditions [110], and PEMWE are characterized by using a solid ion conducting membrane to transport protons from one side of the cell to the other [36]. Each of the mentioned types of water electrolyzers will be briefly described in the following sections.

1.4.2.1. Alkaline water electrolysis

AWE is one of the most established technologies, it was discovered in 1789 by Troostwijk and Diemann [12]. One of its main characteristics is having a liquid alkaline electrolyte, usually 20-30% KOH, but NaCl, NaOH, and H_2SO_4 are also used. The electrolyte allows ions to be transported between the anode and the cathode. Since the electrolyte is a liquid, there is a need of a diaphragm to separate the produced species between the electrodes [2].

This type of electrolyzer operates below 80℃ and 30 Bar and has an efficiency between 25-30%. Figure 2 presents a basic diagram of an AWE. The electrochemical reactions that take place in this type of technology are $2OH^- \rightarrow \frac{1}{2}O_2 + H_2O + 2e^-$ at the anode, and $2H_2O + 2e^- \rightarrow H_2 + 2OH^-$ at the cathode, to give an overall reaction of $H_2O \rightarrow H_2 + \frac{1}{2}O_2$.

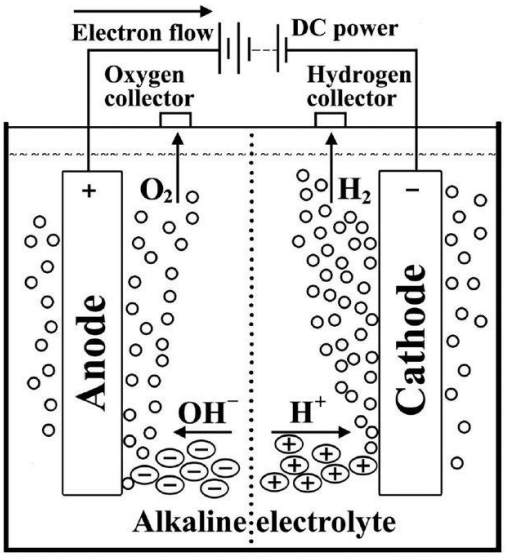

Figure 2. Basic Alkaline Water Electrolyzer (AWE) [69].

The main concerns related to AWE are linked to the operation conditions, for example this type of electrolysis cell can only operate at low current densities, this means it can only

operate at low loads and low pressure. The need of a diaphragm is also a disadvantage since there is a gas crossover through it [8,14,17].

1.4.2.2. Solid oxide water electrolysis

Solid Oxide Electrolysis (SOWE) is characterized for working under high temperatures and can be used for direct conversion of water steam or carbon dioxide into hydrogen and carbon monoxide [28].

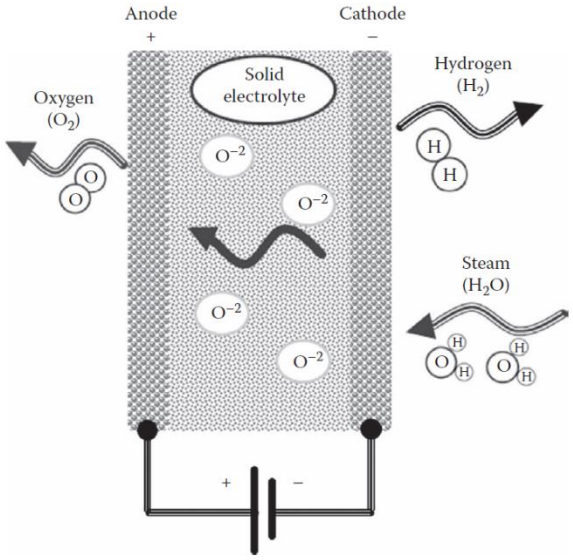

Figure 3. Basic Solid Oxide Water Electrolyzer (SOWE) [9].

When working with steam, the temperature range for this cell is between 500-850 ℃ [37], this has the advantage of using waste heat for the process instead of electricity, increasing the efficiency (60%-70%) compared with the other types of electrolyzers [79] The most common material used for the electrolyte is YSZ (yttria-stabilized zirconia) due to its high ionic conductivity and thermal stability when working under the normal conditions for this type of technology. The electrochemical reactions involved in this process when working with water are

$2O^{2-} \rightarrow O_2 + 4e^-$ at the anode and $H_2O + 2e^- \rightarrow H_2 + O^{2-}$ at the cathode, to give $H_2O \rightarrow H_2 + \frac{1}{2}O_2$ as the overall reaction as shown in Figure 3.

1.4.2.3. Proton exchange membrane water electrolysis

This type of electrolysis cell is characterized by using an ionic conductor membrane. Water is introduced at the anode ($H_2O + Energy \rightarrow H_2 + 12O_2$) and is transported through the Porous Transport layer (PTL) to the Catalyst Layer (CL) where the reaction occurs when a voltage is applied. Water is oxidized to protons, electrons, and oxygen ($H_2O \rightarrow 12O_2 + 2H^+ + 2e^-$).

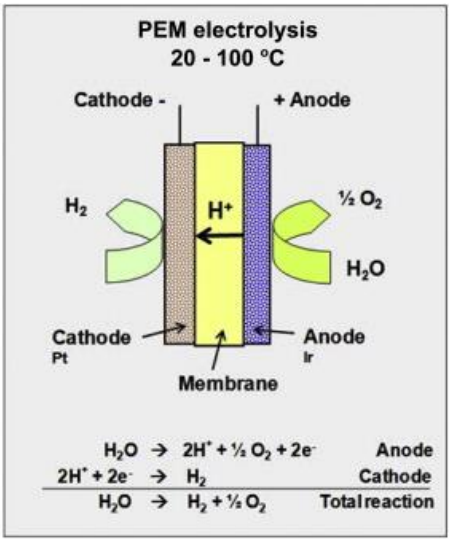

Figure 4. Basic Proton Exchange Membrane Electrolysis Cell (PEMEC) [9,12].

Protons travel through the membrane and electrons travel through the external circuit to be recombined at the cathode ($2H^+ + 2e^- \rightarrow H_2$) to produce hydrogen [8]. Figure 4 shows a simplified schematic of the PEMWE.

1.4.3. PEM electrolysis cell components

An electrolyzer is typically composed of an external power supply, an electrolyte, a membrane, and two electrodes. For the PEM type technology, the components are a Membrane, two Catalyst Layers (CLs), one for each electrode; these two components together are sometimes referred as to Membrane Electrode Assembly (MEA). There are also two Porous Transport Layers (PTL), one for each electrode. Figure 5 illustrates the schematic of a PEMWE including main components and reactions.

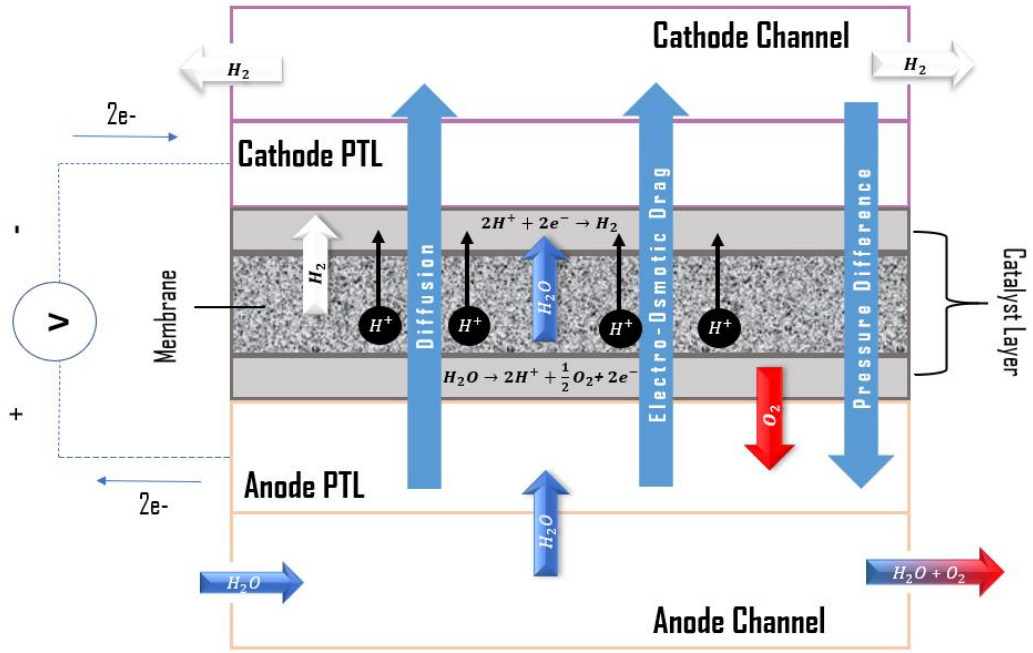

Figure 5. Schematic of a Proton Exchange Membrane Electrolysis Cell (PEMEC).

This type of technology has the advantages of working under high current density (>2A/cm^2), low temperature (80-90°C), and relatively low pressure (<30 Pa), aspects that reduce the operational cost [37]. It can achieve high efficiency (80-90%) [20], a fast response, zero carbon emissions when coupled with renewables, compact design, and a pure hydrogen and oxygen production [18, 25,37,46].

One of the main concerns related to PEMEC is the account of oxygen byproduct in the form of dissolved bubbles present after the OER [74]. since these bubbles can create a blockage in the electrode, adding a mass transport resistance, impeding water to react with the electrocatalyst, and lowering the efficiency of the cell [63].

1.4.3.1. Membrane

The membrane is the most important component of the PEMWE since it provides proton conductivity, keeps the byproducts separated to prevent them getting recombined, allows the cells to work under high pressure, and helps to make the design compact [12]. It is characterized for being a solid polymer, the most common material used is Nafion® since it is found to be mechanical and chemical stable, presents a high proton conductivity when proper conditions are met (hydration state), when working for water electrolysis, the membrane is assumed to be fully hydrated most of the times unless the range of temperature of operation is close to the boiling point, hence its proton commutativity depends on the water content (λ) and the temperature [21]. The thickness of the membrane variates around 0.8 -3 mm [29]. Nafion® also allows the cell to operate at high current density (above $3A/cm^2$), making it possible to achieve high efficiency.

1.4.3.2. Catalyst layer

Catalyst layers are a critical component since here is where the electrochemical reaction of interest occurs [7], hence the CL is responsible of water transportation from the PTL to the CL, electrons transportation from the CL to the PTL, protons transportation from CL the membrane, and oxygen transport from the CL to the PTL [40]. Usually, noble metals like Ir, Pt, Pd and Ru are used as catalyst, but catalysts based on Ru and Ir are the best choices for the anode, due to degradation upon OER [81].

1.4.3.3. Porous transport layer

As its name indicates, PTLs are made from a porous material and are placed at each side of the cell between the membrane and the electrode channels. These layers are responsible for conducting electricity to the CLs and the electrodes, as well as transporting water, hydrogen, and oxygen in and out of the CL area [38]. To perform the above, the PTLs must be chemical stable, need to be able to permit the pass of gas species (byproducts), rigid, the surface of the material is desired to be smooth to avoid electrical resistance between the components of the cell (not being in direct contact), and high electrical conductivity [8]. They are made from highly stable metals, usually titanium-based materials coated with Platinum (anode side) are used due to their resistance in presence of hydrogen, electrical, thermal, and mechanical properties. Carbon-based materials are also commonly used (cathode side) [42].

1.4.4. PEM water electrolysis thermodynamics

The anode (positive) and cathode (negative) are connected by an external power source to form a circuit, when enough potential difference is applied across the water, the positive ions move through the anode and the positive ions move to the cathode, resulting in the formation of oxygen and hydrogen gas at the anode and the cathode respectively [45, 63]. The half-reaction at the anode is called Oxygen Evolution Reaction (OER) and the half-reaction at the cathode is called (HER) and are represented by Eq. (1) and Eq. (2).

$$\text{Anode (OER): } O_{2\,(g)} + 4H^{+}{}_{(aq)} + 4e^{-} \rightarrow 2H_2O_{(l)} \quad (1)$$

$$\text{Cathode (HER): } 2H^{+}{}_{(aq)} + 2e^{-} + 4e^{-} \rightarrow 2H_2O_{(l)} \quad (2)$$

$$\text{Overall: } 2H_2O_{(l)} \rightarrow H_{2\,(g)} + \frac{1}{2}O_{2\,(g)} \quad (3)$$

Since water splitting is a process that requires energy in form of electricity and heat, the theoretical amount of energy required is obtained by the enthalpy of reaction (ΔH_r) [54, 64], that is defined as the energy absorbed or released during a chemical reaction and can be calculated by Eq. (4):

$$\Delta H_r = \Delta G_r + T\Delta S_r \tag{4}$$

Where ΔG_r is the change in the Gibbs free energy and represents the energy that needs to be applied as work and ΔS_r is the change in entropy, that is associated with the thermal energy that is unavailable for doing useful work. When multiplied by the temperature of operation T, represents the thermal energy needed for the reaction to happen.

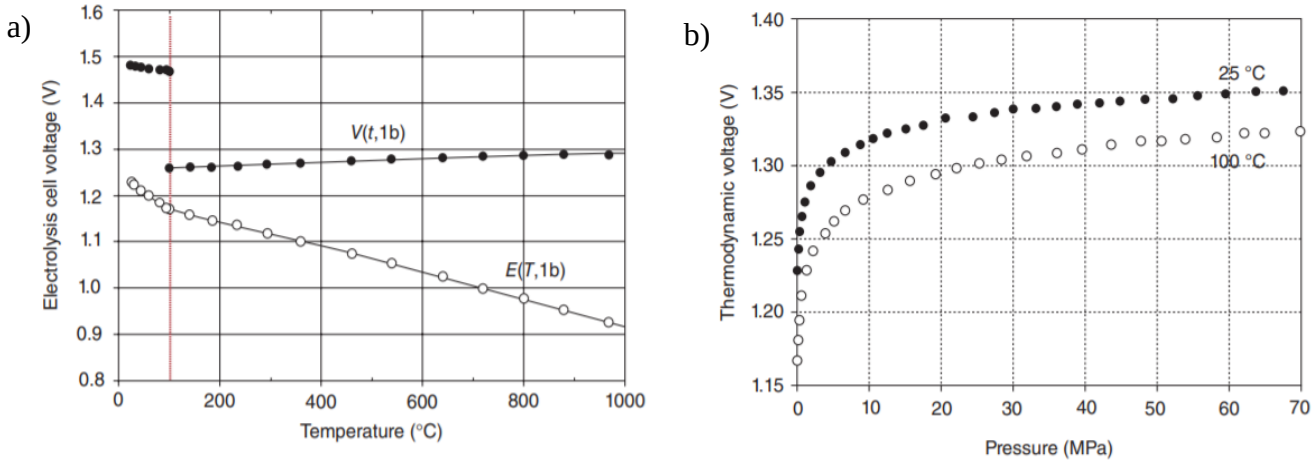

Figure 6. a) Temperature and b) Pressure effects on the voltage of an electrolyzer [24].

For water-splitting reaction, considering both forms of energy and standard conditions (1 atm and 25℃), the potential need would be given by given as [6]:

$$E_{rev} = \frac{\Delta G_r}{nF} = 1.229\ V \tag{5}$$

Where n is the number of electrons transfer during the reaction, and F is the Faraday's constant (96,485 C/mol). This E_{rev} value represents the minimum voltage required for the reaction to take place at the given conditions. If no thermal portion is being provided, the minimum voltage needed would be given by only considering the enthalpy of reaction as [47]:

$$E_{th} = \frac{\Delta H_r}{nF} = 1.481\ V \tag{6}$$

If conditions different than standard are considered, then the energy need is calculated by means of the Nernst equation [8]:

$$E = E_{rev} - \frac{RT}{nF} \ln\left(\frac{P_{H_2O}}{P_{H_2} P_{O_2}^{.5}}\right) \tag{7}$$

Where R is the universal gas constant (8.31447 J/mol K) and P the partial pressure of each of the species involved. Figure 6 shows the effects of temperature and pressure on the voltage need.

1.4.5. Efficiency losses

During operation, current flows across the cell with electrons traveling on the outside and ions traveling on the inside, leading into the above-mentioned Oxygen and Hydrogen Evolution Reactions. Due to different factors like operating conditions, design, and materials, overpotentials occur, increasing the voltage needed to perform the desired reaction. They can be classified as activation (related to the electrochemical reactions at each electrode), ohmic (related to electrons and ions transportation), and mass transport overpotential (related to oxygen removal). These barriers consume part of the energy required for the reaction to happen and that is why they are called overpotentials and the total voltage required from the cell is calculated as the sum of the reversible voltage and the overpotentials mentioned above. Figure 7 shows an

example of a polarization curve for a PEMWE and indicates the predominant region for each overpotential.

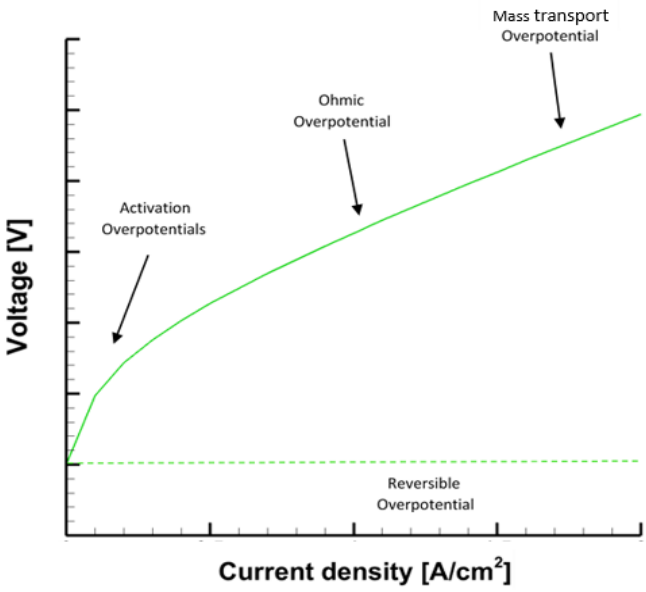

Figure 7. Polarization curve example corresponding to a PEMWE.

The polarization curve evaluation is a widely used method to characterize different types of electrochemical cells, including electrolyzers. It consists of a Voltage (V) vs current density (A/cm^2) plot in most of the cases, but it is usually found in terms of power density (W/cm^2) vs current (A) [43].

1.4.5.1. Kinetics

For the desired chemical reaction to proceed, there is an activation energy barrier that needs to be exceeded and is called activation energy. For PEMEC, the anode activation overpotential tends to be of higher importance than the cathode due to slow kinetics at the anode. Research focuses on reducing the activation energy at the anode, studying the design, materials, and configuration of it. Eq. (8) represents the Butler-Volmer relationship that relates the

overvoltage over the interface of the metal and the electrolyte [63]. It expresses the exponential increase of the current density during an electrochemical reaction, showing that the current generated during the reaction will exponentially increase with exchange current density and the activation overpotential.

$$i = i_0 \left[e^{\left(\frac{\alpha n F \eta}{RT}\right)} - e^{\left(-\frac{(1-\alpha) n F \eta}{RT}\right)} \right] \quad (8)$$

Where i represents the current density in A/cm^2, which can be defined as the current flowing through a cross-sectional area, i_0 is the exchange current density that represents the current at the electrode when it is under equilibrium, η is the overvoltage across the interface, n is the number of electrons transferred during the reaction, α represents the charge transfer coefficient of each electrode, and T the overall temperature of the cell.

1.4.6. Efficiency

The efficiency of the cell is closely related to the cost of the hydrogen produced, the higher the efficiency achieved, the lower the operating cost [68] and can be defined in multiple ways. Since water splitting reaction requires energy, and this requirement is dependent on the operating conditions of the cell, the energy needed for water to get separated into oxygen and hydrogen is usually calculated considering the first and second law of thermodynamics [36]. Several aspects like gas permeation, operating temperature and pressure, thicknesses of the membrane and electrodes, current density, losses, among other particularities need to be considered when the cell is analyzed as a part of a system. The following sections describe the efficiency in terms of Faradic and voltage efficiencies.

1.4.6.1. Faradic efficiency

The Faradic efficiency stayed in Eq. (9) is used when gas diffusion and leakage are considered, as well as corrosion and oxidation, hence it is dominated by gas crossover [37,64] affecting the hydrogen production compared with ideal conditions when no mass transfer is assumed.

$$\eta_F = \frac{\dot{m}nF}{IM_{H_2}} \tag{9}$$

Where $\dot{m}$ represents the mass flow rate and M_{H_2} is the hydrogen mass. It describes the ratio between the actual amount of hydrogen generated and the theoretical hydrogen that could be produced based on the electrical input [88].

1.4.6.2. Voltage efficiency

This efficiency relates the thermoneutral potential to the actual voltage of the electrolysis cell as indicated in Eq. (10). It considers mass transport losses, as well as ohmic and activation losses accounted in the actual voltage of the PEMEC (V_{cell}) [5], losses that will be covered later during chapter 2. Changes in pressure and temperature also impact the voltage efficiency, since these conditions will affect the thermodynamical voltage required [72].

$$\eta_E = \frac{E_{rev}}{V_{cell}} \tag{10}$$

1.4.6.3.Overall efficiency

The overall efficiency of the electrolyzer is calculated using Eq. (11) that considers both, Faraday and voltage efficiencies [72] since aspects like the imperfect contact between the components where the reactions take place, oxygen bubbles blocking the CL, and side reactions that do not produce hydrogen but consume energy need to be considered.

$$\eta_{Cell} = \eta_F \eta_E \quad (11)$$

1.5. Previous work and contribution of the present work.

Several studies have focused on the experimental investigation of PEMEC, nevertheless, modeling represents a very powerful tool to understand the behavior of this type of system to achieve cost-effective solutions to increase the performance of PEMEC. Previous modeling works have tried to adapt the well-studied PEMFC models to PEM water electrolysis [10,91,92,93,94], however, most of the studies recurred to simplified modeling and considerations (0-D approximations considering low current densities, low operating temperature and pressure, no detailed mass transport, no heat transfer, etc) to obtain fairly accurate results. Busquet *et al.*, (2004) [10] proposed a very classical and simplified semi empirical model that didn't consider the effect of diffusion or thermal degradation. The model proved to satisfactory reproduce experimental data when working under low current density, but it was not useful to prove the effects of high pressure due to its nature. Kim *et al.*, (2013) [35] introduced a 1-D dynamic model working under high-pressure conditions integrating gas permeation, volume variation, compressibility, water transport, and vaporization. The results revealed that the dynamics at the anode and the cathode are fast and slow respectively due to the fluid velocity, that operating under low current density and flow rate, and high pressure cause an increase in the hydrogen concentration.

Later works started to address higher complexity models, like Marangio *et al.* (2009) [44] who contributed with a semi-empirical model considering high-pressure operation and its effect on the voltage losses and resistances between the cell components, to do this, the authors incorporated a thermodynamic analysis. Their work was extended to the construction of a prototype that was tested under different pressure (1-7 MPa) and temperature (40°C, 48°C, and

55℃) conditions. Particular attention was paid to the dependence of the cathodic exchange current density and the diffusion coefficient of hydrogen protons in the membrane. Schalenbach *et al.*, (2013) [72] also considered the influence of high operating pressure (up to 30 bar) and its correlation with the Faraday efficiency (gas crossover) by studying the dependency of the membrane thickness, conductivity, permeability, current density, and the pressure of the electrode. The authors were able to come with a computational model used to optimize the membrane conditions based on the operating pressure.

Merrill, (2007) [45] suggested a mathematical model incorporating physical and empirical approaches from previous works, mostly considering the cell electrochemical reaction dynamics. The performance of the cell was evaluated under a range of temperatures (50℃-80℃) at low current densities (up to 2A/cm^2). Their main contribution was to define an efficiency relationship in terms of temperature. Results showed that at low current densities, the first principle of efficiency reached values higher than 100%, and at higher energy density values, the efficiency started to decrease due to heat dissipation.

Several papers evaluate the PEMEC performance under current densities up to 2 or 3A/cm^2 [1,2,10,11,12,13,27,39,44,85] to simplify the modeling process avoiding some forms of mass transport losses. As stayed by Faraday's law, the increase in current density also increases gas production [4], leading into formation of oxygen nano-bubbles. This nano-bubbles can impede water to react at the CL, reducing the performance of the cell [32]. Fritz *et al.* (2014) [22] presented one of the first models capable of analyzing the effects of mass transport at high current densities (2-6 A/cm^2). Ojong *et al.* (2017) [59] proposed a new design without flow channels in the bipolar plates (BP). They developed a semi-empirical model that quantified the effect of the bubble coverage at the cathode. Their analysis contemplated the operation at high

current densities up to 5 A/cm^2 and neglected the effects of the contact resistance between the cell components. It was determined that the PTL properties (like pore size and thickness) are critical parameters to reduce the mass transport limitations when working under this non-conventional design.

A contribution considering high current density was made by Saebea *et al.* (2017) [70] who determined working under high pressure and high current density (15000 A/cm^2) increases the gas crossover. The authors analyzed the effect of the membrane thickness to reduce the gas leakage, concluding that the use of a thicker membrane reduces the cell performance. Oliveira *et al.* (2013) [56] contributed with a multi-scale transient model considering the kinetics and a non-equilibrium behavior of the nanoscale catalyst–electrolyte interface. This work analyzed the performance of the cell at different operating conditions and catalyst loadings. The mathematical model consisted of a 1-D mass transport approach that was validated against experimental data taken at different temperatures (17℃-107℃).

Chen *et al.* (2020) [13] used a 2-D multi-physics model to account for two-phase flow, electron/proton transfer, mass transport, and water electrolysis kinetics on the PTL and the Channel -Land structure. The model coupled charge conservation equations for protons and electrons with electro-kinetics and mass and momentum conservation for liquid and gas phases. This model was used to study the impact of the PTL thickness (100µm, 200µm, and 500µm) and local current density on liquid water saturation. Their study concluded that derived from the OER at the anode, water saturation decreases from the flow channel to the CL and from the channel to the land (considering the plane direction). At conditions where the thickness of the PTL is 100µm and current density higher than 4A/cm^2, the water saturation showed to be low, increasing the overvoltage about 0.2 V at 5A/cm^2.

Though many modeling studies have been attempted, few works considered a two-phase mixture in the PTL and channel and the interfacial resistance at the PTL surface, along with validation against various experimental data. The aim of the present work is to study the contribution of the different voltage losses to the polarization curve under different current density, pressure, temperature, and liquid saturation percentages. The study proposes a cell level PEMEC model that has been tested against available literature data. Basic electrochemical and mass transport phenomena related to water electrolysis have been simulated using MATLAB/Simulink considering some specific properties of the electrodes and the membrane along with operating conditions.

Chapter 2-Mathematical modeling

This chapter presents a model for PEMEC voltage losses taking place during water splitting reactions considering the following assumptions: 1.) isothermal conditions, 2.) cathode transport loss is neglected, 3.) electrochemical reaction kinetics are approximated by the Tafel equation, and 4.) homogeneous properties in each component. The model is divided into four main sections: PEMEC Voltage, Anode Side, PEM, and Cathode Side, and the components modeled are shown in Figure 8 along with the formulas used on each section. Each of the MATLAB/Simulink modules of the diagram interact with each other and are designed to be run separately.

The model first describes the overall voltage of the PEMEC at the PEMEC voltage section, considering the minimum necessary voltage for the reaction of interest to take place along with the main voltage losses related to the process. The subsequent section Anode side indicates how to calculate the water flows and fluxes at this side of the cell, considering vapor

and liquid fractions. This section also includes the interfacial sub-model at the PTL/Channel interface that takes into account the influence of the mass transport overpotential (liquid water saturation) at the PTL. The following section named PEM, covers the water transport at the membrane, considering diffusion, electro-osmotic drag (EOD), and water movement due to pressure differences between the anode and the cathode. Finally, the last section called cathode calculates the mass balance at this side of the PEMEC considering the relevant species present.

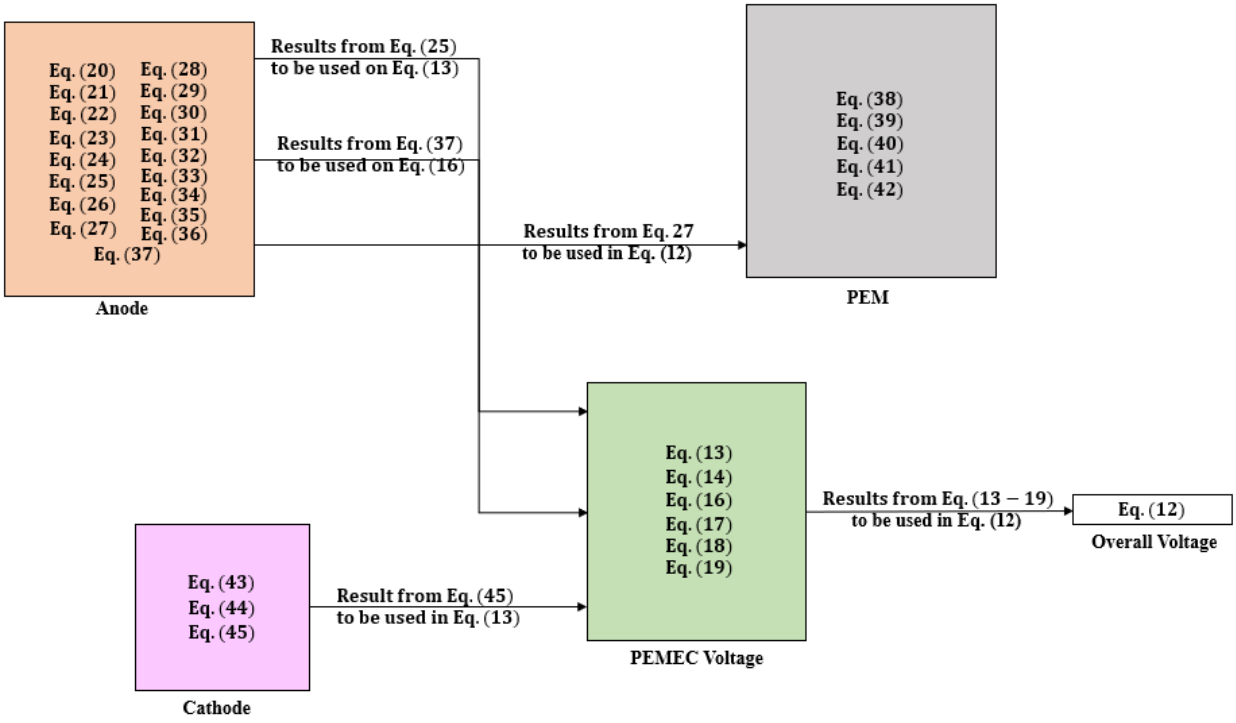

Figure 8. Diagram indicating the equations used at each block of the MATLAB/Simulink model.

2.1. PEMEC voltage

The operating voltage (E) of an electrolyzer is calculated as the sum of the Nernst voltage and three overpotentials, ohmic, activation, and transport (V_{ohm}, V_{act}, and V_{con}) [1,39,44, 85]:

$$E = V_{oc} + V_{act} + V_{ohm} + \mathrm{V}_{con} \tag{12}$$

Where V_{oc} represents the open circuit (OC) voltage, assuming it is the same as the reversible voltage of the cell, and is defined as the necessary external energy demand [1,45]:

$$V_{oc} = E_0 + \frac{RT}{2F}\ln\left(\frac{P_{H_2}P_{O_2}{}^{.5}}{a_{H_2O}}\right) \tag{13}$$

The water activity a_{H_2O} is equal to one since liquid water is fed the cell. E_0 represents the maximum amount of electrical work needed without losses when working under standard conditions [8,39]:

$$E_0 = \frac{\Delta G^{\circ}}{2F} \tag{14}$$

The activation overpotential V_{act} accounts for the loss (electrons transference) related to the kinetics of the OER and HER reactions taking place at the surface of each electrode. It can be evaluated using the following formula based on the Butler-Volmer equation [1,23,39,44,85]:

$$V_{act} = \frac{RT}{F\alpha_c} sinh^{-1}\left(\frac{i}{2i_{0,c}}\right) + \frac{RT}{F\alpha_a} sinh^{-1}\left(\frac{i}{2i_{0,a}}\right) \tag{15}$$

Where α_c and α_c represent the charge coefficient of each electrode (cathode and anode respectively). Eq. (15) was modified to take the liquid water saturation s_0 at the anode CL/PTL interface as:

$$V_{act} = \frac{RT}{F\alpha_c} sinh^{-1}\left(\frac{i}{2i_{0,c}}\right) + \frac{RT}{F\alpha_a} sinh^{-1}\left(\frac{i}{2i_{0,a}s_0}\right) \tag{16}$$

The details related to water saturation are described in the section of “Anode side”. The Ohmic overpotential occurs due to the ohmic resistance in the membrane and between the cell

components (*i.e.* contact resistance). Assuming the contact resistance is negligible, it can be calculated using Ohm's Law [1] as:

$$V_{ohm} = \frac{\delta_{mem}}{\sigma_{mem}} i \tag{17}$$

Where δ_{mem} represents the membrane thickness. Since the material used at the membrane is Nafion®, its conductivity σ_{mem} is treated as a function of the water content and temperature [67]:

$$\sigma_{mem} = (0.005139\lambda - 0.00326) e^{\left(1268\left(\frac{1}{303} - \frac{1}{T}\right)\right)} \tag{18}$$

The concentration overpotential, is driven by a change in the concentration of the reactants at each electrode (like that in fuel cells) [82]. It can be estimated by the concentration of gaseous species in the electrodes or at the membrane surface ($C_{O_2}^{mem}$ and $C_{H_2}^{mem}$) and a reference position ($C_{O_2,mem}^{0}$ and $C_{H_2,mem}^{0}$) following [1,39,44]:

$$V_{con} = \frac{RT}{4F} ln\left(\frac{C_{O_2}^{mem}}{C_{O_2,mem}^{0}}\right) + \frac{RT}{2F} ln\left(\frac{C_{H_2}^{mem}}{C_{H_2,mem}^{0}}\right) \tag{19}$$

2.2. Anode side

As mentioned before, water is pumped to the anode and when a voltage is applied, an OER takes place. Oxygen is produced on the anode side while protons and electrons travel through the membrane and the external circuit to the other side of the cell [37]. Therefore, the water mass balance in the anode side can be developed by [1,39]:

$$\dot{N}_{H_2O} = \dot{N}_{H_2O,in} - \dot{N}_{H_2O,cons} - \dot{N}_{H_2O,vapor} - \dot{N}_{H_2O,eod} \tag{20}$$

As shown in Eq. (20), liquid water ($\dot{N}_{H_2O,in}$) is inputted to the anode side: part of which is consumed ($\dot{N}_{H_2O,cons}$)during the process and part dragged through the membrane ($\dot{N}_{H_2O,eod}$) by electro-osmotic drag (EOD). Part is also vaporized into gas phase ($\dot{N}_{H_2O,vapor}$).

Using Faraday's Law, the amount of water consumed can be calculated using Eq. (21) [1,39]:

$$\dot{N}_{H_2O,cons} = \frac{i}{2F}, \text{ where } I = \frac{i}{A} \tag{21}$$

Once the reaction takes place, the oxygen generated can be calculated by [1,39,44,85]:

$$\dot{N}_{O_2,gen} = \frac{i}{4F} \tag{22}$$

The Oxygen flux rate at the anode is equivalent to the oxygen generated rate per unit area [1,34,85]:

$$\dot{N}_{O_2} = \dot{N}_{O_2,gen} \tag{23}$$

Following [16,39], water vapor saturation pressure is assumed to be temperature dependent and is calculated using Antoine's equation:

$$P_{H_2O,sat} = 10^{8.07131 - \frac{1730.63}{233.426+T}} \tag{24}$$

Hence, the partial pressure of oxygen P_{O_2} can be obtained as the difference between the total pressures of the anode minus the saturated pressure of water vapor ($P_{H_2O,sat}$) using Dalton's law [1,85]:

$$P_{O_2} = P_a - P_{H_2O,sat} \tag{25}$$

The volumetric flow rate of liquid water ($\dot{\forall}_{H_2O,l}$) at the anode outlet can be calculated considering the total flow rate of water at the outlet, molar mass, and density of water:

$$\dot{\forall}_{H_2O,l} = (\dot{N}_{H_2O,\,in} - \dot{N}_{H_2O,\,cons} - \dot{N}_{H_2O,\,vapor} - \dot{N}_{H_2O,\,eod})\frac{M_{H_2O}}{\rho_{H_2O}} \tag{26}$$

Where $\dot{N}_{H_2O,vapor}$ can be calculated considering the oxygen flow, pressure, and the water-vapor pressure at the anode:

$$\dot{N}_{H_2O,vapor} = \frac{\dot{N}_{O_2} P_{H_2O,sat}}{P_{O_2}} \tag{27}$$

Using the ideal gas law, the volumetric flow rate of oxygen ($\dot{\forall}_{O_2}$) and water vapor ($\dot{\forall}_{H_2O,\,vapor}$) can be calculated as:

$$\dot{\forall}_{O_2} = \frac{\dot{N}_{O_2} RT}{P_{O_2}} \tag{28}$$

$$\dot{\forall}_{H_2O,\,vapor} = \frac{\dot{N}_{O_2} RT}{P_{H_2O,sat}} \tag{29}$$

The volumetric fraction of liquid water ($\varphi_{H_2O,l}$) at the outlet can be then calculated by using the volumetric flow rate of the gaseous species involved as:

$$\varphi_{H_2O,l} = \frac{\dot{\forall}_{H_2O},\,l}{\dot{\forall}_{H_2O,l} + \dot{\forall}_{H_2O,\,vapor} + \dot{\forall}_{O_2}} \tag{30}$$

Finally, assuming liquid water and gas are homogeneously mixed in the channel [97], the gas volume fraction at the outlet can be obtained by:

$$\varphi_{O_2} + \varphi_{H_2O,\,Vapor} = 1 - \varphi_{H2O,l} \tag{31}$$

Liquid water saturation is defined as the volume fraction of liquid relative to the pore volume or void space [90], which is similar to that in PEM fuel cells [99,102].

For a 1-D problem, the below solution is reached considering the PT/CL interface at x=0 and PTL/ channel interface as x=200μm [103]:

$$\frac{I}{2F} M_{H_2O} = \frac{k_{rl}}{\nu} K \nabla p_c \tag{32}$$

Where p_c is the capillary pressure, K represents the permeability in m^2, ν the kinematic viscosity of water, and liquid saturation, K represents the permeability in m^2, ν the kinematic viscosity of water, and k_{rl} is the relative permeability of the liquid phase. The approach considers a steady state flow in the through-plane direction, assuming the capillary action as the main driving force for liquid flow yields. Substituting the Leveret function into Eq. (32) leads to:

$$\frac{1}{2F} M_{H_2O} = -\frac{s^3}{\nu} K \sigma \cos\theta_c \left(\frac{\varepsilon}{K}\right)^{1/2} \nabla J(s) \tag{33}$$

Where s is the liquid saturation, σ stands for the surface tension, θ_c is the contact angle of the PTL, ε the electrode porosity, and $J(s)$ is the Leverette function. Considering a hydrophilic GDL, the J function takes the form [13]:

$$J(s) = 1.417(1-s) - 2.120(1-s)^2 + 1.263(1-s)^3 \tag{34}$$

Then the solution to Eq. (34) will give:

$$s^4(-0.2415 + 0.6676s - 0.6135s^2) = \frac{I}{2F} M_{H_2O} \frac{\nu}{\sigma \cos(\theta_c) \sqrt{\frac{\varepsilon}{K}}} x + C_1 \tag{35}$$

Where C_1 is a constant of integration determined by the boundary conditions.

2.3. Interfacial sub-model at the PTL/Channel interface

Mass transport related overpotentials have been gaining attention due to the lack of understanding of the phenomena since the processes related are of a high complexity. The

following sub-model intents to help to understand the influence of the mass transport overpotential at the PTL. In this case, the study of interest is the liquid water saturation at the anode PTL surface s_0 or the oxygen area fraction covering the PTL surface (1-s_0) as shown in in Figure 9.

Considering convective mass transfer the transport of material between a moving fluid and a boundary surface [52,104] (bulk movement of a fluid), it is assumed that the oxygen bubble removal at the PTL surface follows the species convective transport at a solid/fluid interface:

$$S_{O_2} = h_{mass}(C_{O_2} - C_{O_2,bulk\ flow}) \tag{36}$$

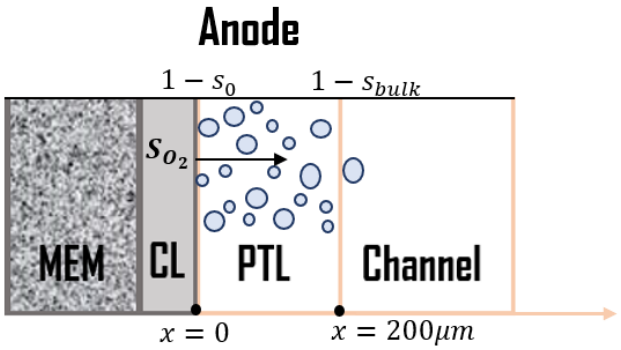

Figure 9. Schematic diagram of the anode side indicating the liquid saturation position in the PTL.

Where h_{mass} represents the mass-transfer coefficient that is related to the geometry of the system analyzed, the properties of the fluid, and the characteristics of the flowing fluid [70]. In Eq. (36), S_{O_2} is equal to $\frac{i}{4F}$. Because the oxygen volume fraction is equal to $1 - s$, the below equation can be established at the PTL/Channel interface, relating the surface liquid fraction to the current density i:

$$s_0 = iC + C_0 \tag{37}$$

Where C and C_0 are i-independent parameters, determined by the oxygen bubble adhesion on PTL surface and drag by the water flow. Note that the two forces are related to the surface wettability, pore size, and channel water velocity. In this study, we consider C_0=1, *i.e.* the liquid fully occupies the PTL surface when there is no oxygen production.

2.4. PEM

As previously mentioned, water can be transported between the anode and the cathode sides due to the following phenomena: diffusion, electro-osmotic drag (EOD), and pressure difference between electrodes, hence the water flow through the membrane can be calculated as [1,8, 39, 44]:

$$\dot{N}_{H_2O,mem} = \dot{N}_{H_2O,Diff} + \dot{N}_{H_2O,eod} - \dot{N}_{H_2O,Pe} \tag{38}$$

Water diffusion occurs due to a concentration with the diffusive rate given by [1,8,11,39, 44]:

$$\dot{N}_{H_2O,Diff} = \frac{ADw}{\delta_{mem}}\left(C^{c}_{H_2O,mem} - C^{a}_{H_2O,mem}\right) \tag{39}$$

The water flux due to EOD is related to the movement of protons in the ionomer phase [44], which can be calculated using the following equation [1, 4,15,16]:

$$\dot{N}_{H_2O,\,eod} = \frac{n_d I}{F} \tag{40}$$

Where n_d represents the electro-osmotic drag coefficient. This coefficient depends on the water content as [13]:

$$n_d = \begin{cases} 1.0 \; for \; \lambda \leq 14 \\ \frac{1.5}{8}(\lambda - 14) + 1.0 \; otherwise \end{cases} \quad (41)$$

Some of the liquid water from the cathode permeates across the membrane to the other side of the cell when there is a total pressure gradient. This water transport $\dot{N}_{H_2O,Pe}$ is estimated by [1,2,7,18,56]:

$$\dot{N}_{H_2O,Pe} = \frac{(K_{Darcy}\rho_{H_2O}\Delta P)}{M_{H_2O}\mu_{H_2O}\delta_{mem}} \quad (42)$$

In this work, symmetric pressure between both electrodes is assumed, hence $\dot{N}_{H_2O,Pe}$ is considered to be zero.

2.5. Cathode side

Protons and electrons arrive at the cathode after traveling through the PEM (proton conductive) and the external circuit respectively, to be recombined to produce hydrogen [37]. Thus, the mass balance in the cathode needs to consider the generated hydrogen and the amount of hydrogen going in and going out of the cell [1,39,44,85]:

$$n_d\dot{N}_{H_2} = \dot{N}_{H_2,in} - \dot{N}_{H_2O,out} + \dot{N}_{H_2,gen} \quad (43)$$

Generated hydrogen can be obtained using a similar approach as for the oxygen at the anode side and is calculated as follows [1,37,44,85]:

$$\dot{N}_{H_2,gen} = \frac{i}{2F} \quad (44)$$

Finally, the partial pressure of hydrogen at the cathode can be calculated as [44, 85]:

$$P_{H_2} = P_c - P_{H_2O,sat} \tag{45}$$

Figure 10 shows the Simulink model of the PEM water electrolysis cell. Which considers the anode, cathode, and PEM for the PEMEC voltage prediction.

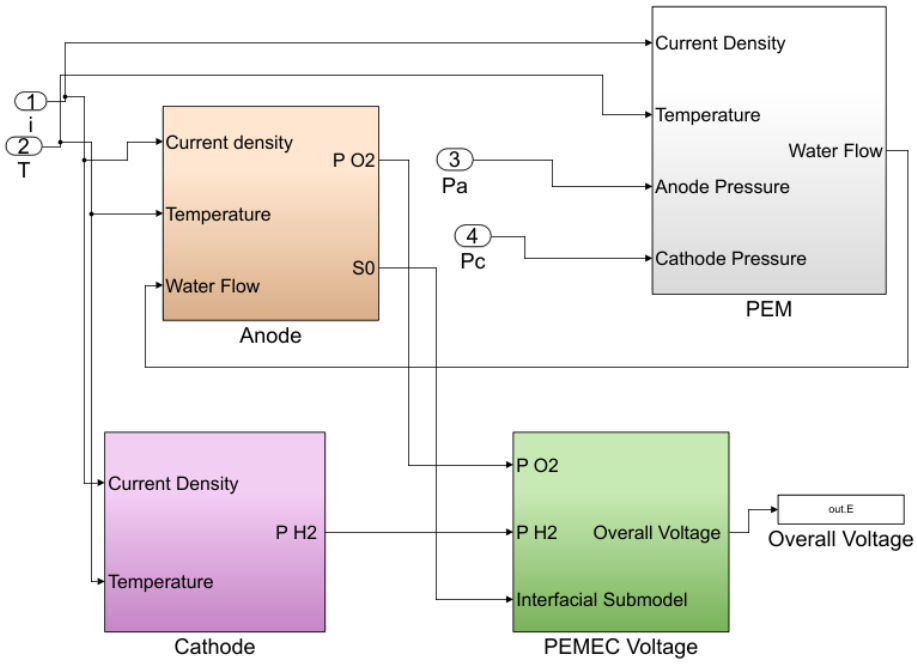

Figure 10. Simulink Model of a PEMEC system.

Chapter 3- Results and discussion

This study is focused on the influence of different current densities, pressure, temperature, and liquid saturation percentages to the voltage losses of the cell and its contribution to each section of the polarization curve to evaluate the importance of each the parameters considered for the simulation. The software selected for the simulation was MATLAB/Simulink. First, the simulation was carried at normal current density operation (0 to 2A/cm^2 and fixed temperature and pressure of 80°C and 1 bar respectively to validate it against

the extensive data available in the literature. Three different values of $\boldsymbol{s_0}$ where used for to evaluate its influence in the voltage of the cell. After comparing the obtained results with the literature, the best fit selected was $s_0 = 0.45$. After confirming the validity of the model, it was tested under high-current density (0 to 5A/cm^2) and same conditions of temperature and pressure as the previous case. The influence of high current density under fixed pressure and temperature to each region of the polarization curve was analyzed. Finally, the model was used to evaluate the impact on the cell voltage when working under high current densities, and different temperature and pressure.

3.1. Water saturation at the PTL surface

Figure 11a and 11b show the polarization curves recorded when working between 0 to 2 A/cm^2 and 0 to 5 A/cm^2 respectively. Both cases were run under 80°C and 1 bar and considering three different values of water saturation at the PTL surface. Table1 lists different values of $\boldsymbol{s_0}$ at its corresponding current density for $s_0 = 0.45$, $s_0 = 0.40$, and $s_0 = 0.35$ respectively.

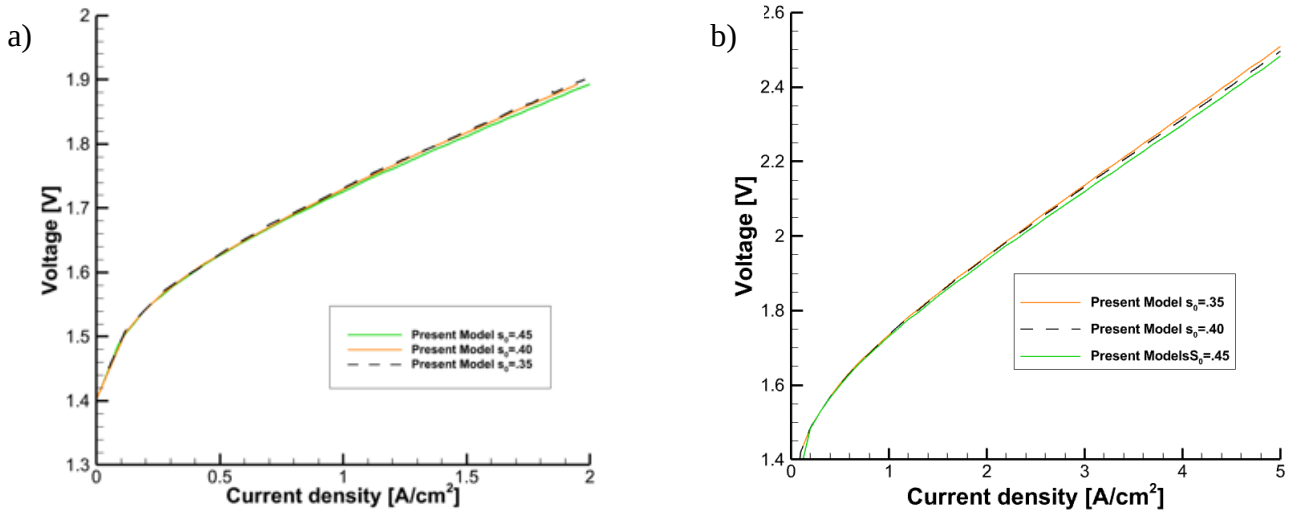

Figure 11. Polarization curve considering three different s_0 values when working at a) 0-2A/cm^2 and b) 0-5A/cm^2

The influence of the saturation value is attributed to the formation of bubbles that is hard to describe under this model. For all the three cases, a fully liquid water saturation state wasassumed until reaching the above values defined for s_0.

As shown in Figure 11a and 11b, the simulated data using a value of $s_0 = 0.35$ resulted on voltages accounting for ~1.9 V and ~2.5 at 2A/cm^2 and 5A/cm^2 respectively. For the value of $s_0 = 0.40$ voltages turned ~1.89V and ~2.49V at 2A/cm^2 and 5A/cm^2 respectively. Finally, when working with an $s_0 = .45$, the voltage reached was ~1.894V and ~2.48V at 2A/cm^2 and 5A/cm^2.

Table 1. Numerical values for water saturation a) $s_0 = 0.45$, b) $s_0 = 0.40$ and c) $s_0 = 0.35$at the PTL surface.

a) $s_0 = iC + C_0$, where $C = 1.595x10^{-5}$and C_0=1		b) $s_0 = iC + C_0$, where $C = 1.3x10^{-5}$and C_0=1		c) $s_0 = iC + C_0$, where $C = 1.2x10^{-5}$and C_0=1	
Current density (A/cm^2)	Water saturation at the PTL Surface (s_0)	Current density (A/cm^2)	Water saturation at the PTL Surface (s_0)	Current density (A/cm^2)	Water saturation at the PTL Surface (s_0)
0	1	0	1	0	1
1	0.89	1	0.88	1	0.87
2	0.78	2	0.75	2	0.74
3	0.67	3	0.64	3	0.61
4	0.56	4	0.52	4	0.48
5	0.45	5	0.40	5	0.35

According to Eq. (16), the effect of water saturation is accounted in the activation overpotential at the anode side, hence the rest of the voltage losses remain the same as inferred from Figure 12 where the contribution of each voltage loss is presented. It can be observed that the difference between the three runs when analyzing the anode activation overpotential is about 1%.

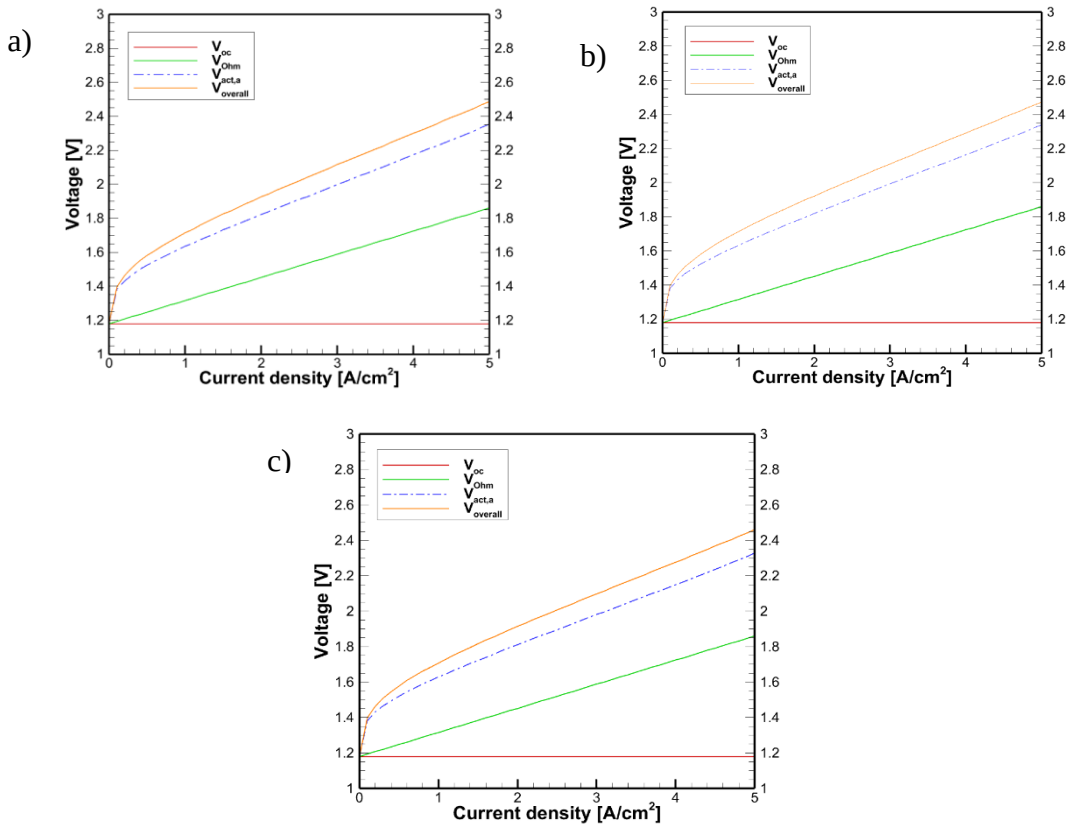

Figure 12. Contribution to the different voltage losses considering a) $s_0 = .35$, b) $s_0 = .40$, and c) $s_0 = .45$.

After analyzing the results, a saturation of 0.45 was selected to be included on the model. This seems to be reasonable when compared with the data provided by [13] that proved to have a water saturation between 0.4 and 0.45 when working at high current density and a PTL thickness between 200µm and 500µm due to the formation of oxygen bubbles blocking the space of the CL where the reactions of interest take place.

3.2. Normal current density

Once the s_0 value to be used in the model is defined assuming fully liquid water saturation state ($s_0 = 1$), until reaching a value of 0.45 at 5A/cm^2, the obtained information was validated using the experimental data obtained by [13], [71], and [95] under a range of current

density from 0 to 2A/cm^2 at 80°C as shown in Figure 13. The results were modeled considering a PTL and membrane thicknesses of 200µm [59,80].

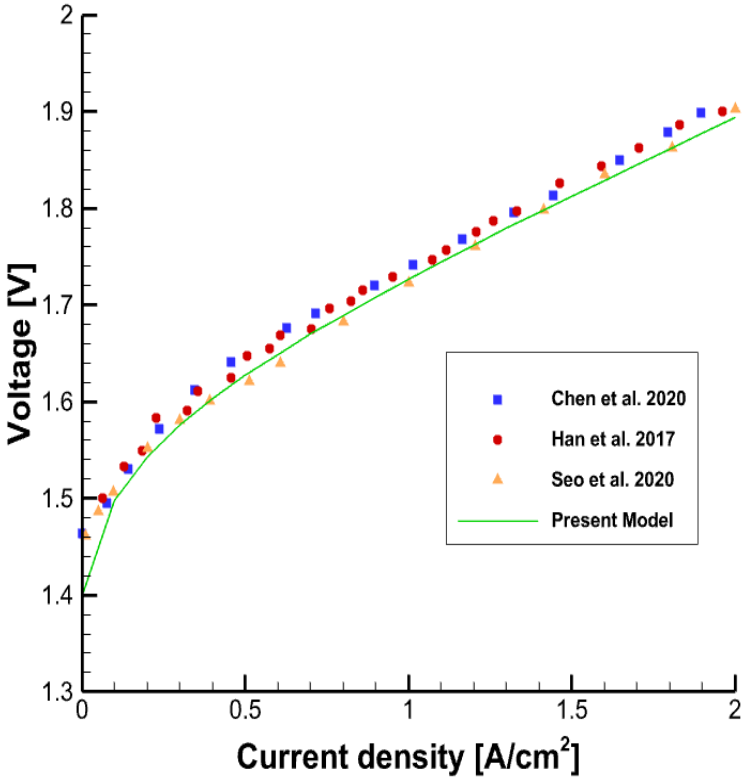

Figure 13. Polarization curve (0-2A/cm^2) comparison @80°C and 1 bar

Pressure was set to 1 bar and a porosity of 0.3 was considered [1,44] since are common experimental conditions found in the literature. Results show a good agreement with the information provided by Chen *et al.* (2020), Han *et al.* (2017), and Seo *et al.* (2020) [13,39,95]. Figure 13 shows a logarithmic trend due to the contribution of the different losses explained by Eq. (12) to Eq. (19), primally due to the influence of the ohmic and activation overpotentials accounting for ~0.25 V and ~0.44 V respectively at 2A/cm^2. Ohmic and activation losses are dependent on the current density, the higher the greater the losses due to an ohmic resistance between the cell components, same case with the activation losses due to the formation of gas bubbles. However, this last overpotential is also influenced by the operating temperature, the

higher the temperature the lower the losses. The effect of temperature is discussed later in section 3.3. Since Figure 13 presents the results when the PEMEC is working between 0 and 2A/cm^2, the voltages reached are smaller than the ones presented in the following sections when the model is being evaluated under high current density and the influence of its effect is greater.

3.3. High current density operation

As mentioned before, the operation under higher current densities (>3A/cm^2) is desirable as it leads to a higher rate of hydrogen produced per area or catalyst loading. Figure 14 presents the validation of the present model working from 0 to 5A/cm^2.

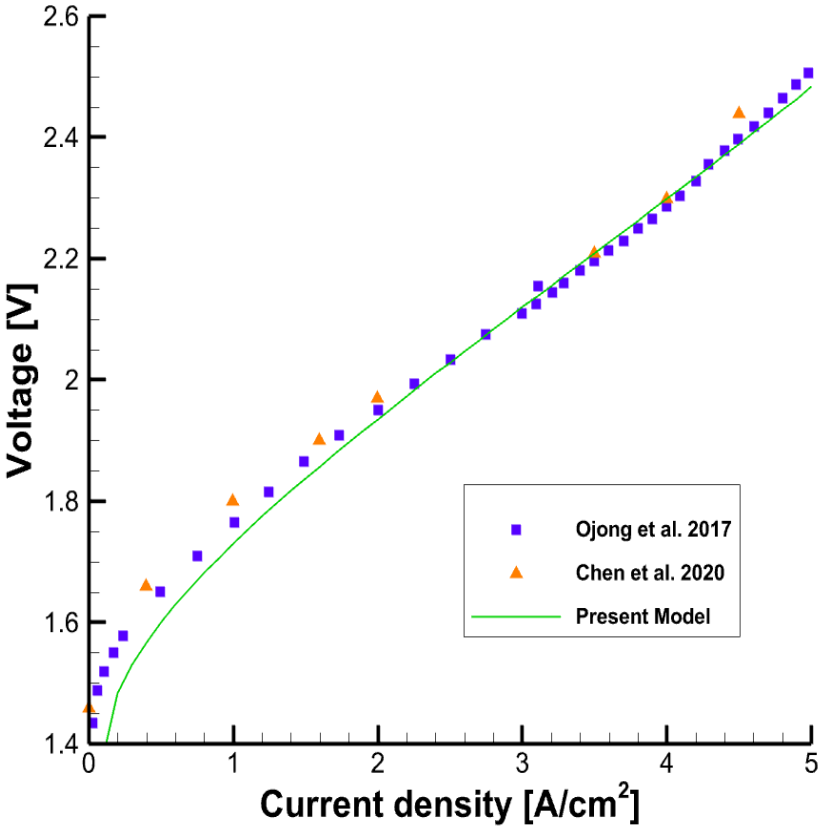

Figure 14. Polarization curve (0-5A/cm^2) comparison @80°C and 1 bar.

It is simple to determine that the higher the current density the higher the overall voltage of the cell. For higher current density, there is a greater need for overpotential at the reaction interface to drive the reaction rate. It is seen that the cell voltage increase accelerates slightly after 3-4A/cm^2. At 3A/cm^2, the electrolyzer reached a voltage of ~2.20V, at 4A/cm^2, it achieved ~2.30V. Finally, when working at 5A/cm^2, the calculated voltage was ~2.48V. This may be related to the mass transport limitation in the PTL and bubble removal resistance at the PTL/Ch interface.

For operation at high current densities, the formation of bubbles is faster, leading to a large bubble coverage at the PTL/Ch interface and consequently lower accessibility of liquid water to the CL. In addition, a higher current density will raise the liquid saturation drop from the PTL/Ch to the CL, as shown in Eq. (37), which causes a lower liquid water content in the CL as refered in Figure 15 and larger voltage loss.

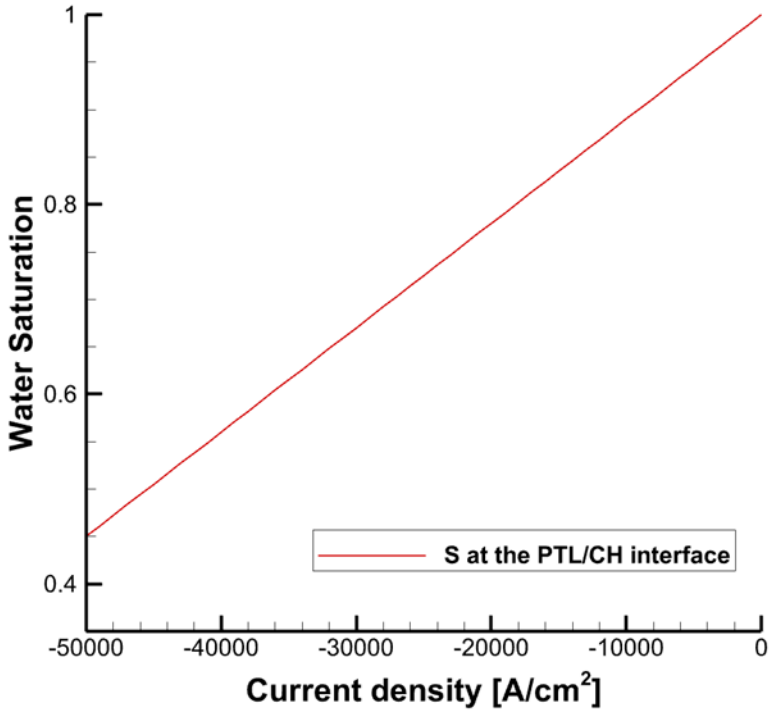

Figure 15. Water saturation profile at different current densities.

In Chen *et al.* (2020) [13], they show that part of the PTL and CL under the land is subject to very low liquid water content, which significantly raises the voltage loss. Figure 16 shows the overpotentials due to the Nernst voltage (Voc), proton transport through the PEM (ohmic), and electrode reaction kinetics (activation). The ohmic overpotential, marked in green is one of the highest contributors to the cell voltage, reaching ~0.68V at 5A/cm^2, representing 27% of the total voltage. When comparing the results of the present model with the ones obtained by Ojong *et al.* (2017) [59], an increment of the activation overpotential can be seen at high current density, this can be explained by the gas saturation increment considered at the anode.

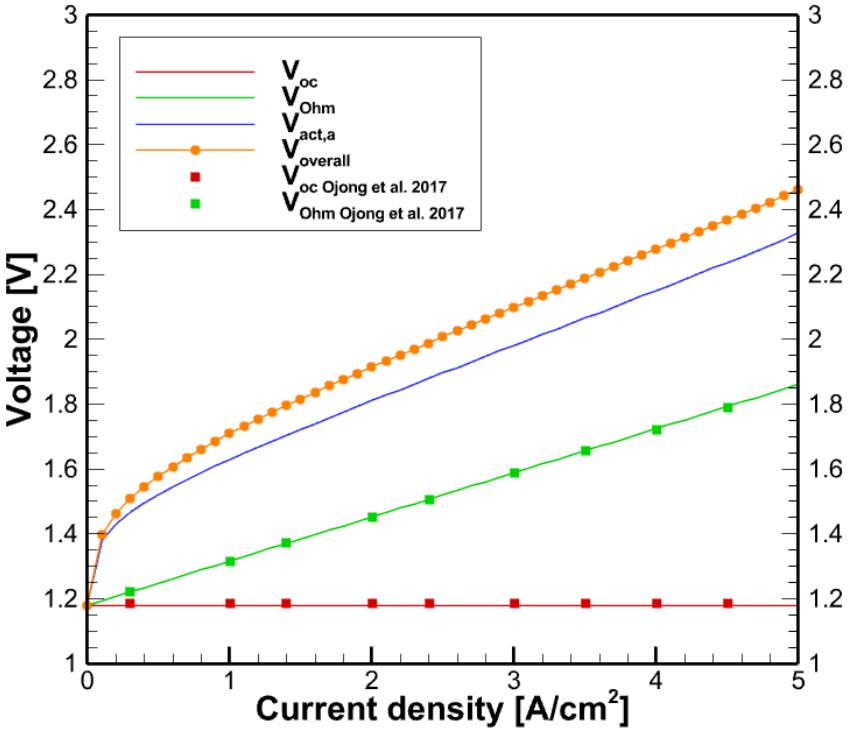

Figure 16. Influence of the different overpotentials (0-5A/cm^2) @ 80°C and 1 bar.

At 3A/cm^2, the gas saturation $1 - \dot{s_0}$ is estimated to be ~0.33, contributing to the activation overpotential increment of approximately 7% compared to the authors. A similar trend is obtained at 4A/cm^2 and 5A/cm^2 where the oxygen saturation near the PTL surface is 0.44 and

0.55 respectively, making the activation losses increase ~8% and ~10% respectively. Figure 16 also shows that the Nernst Voltage represents around 68% of the total voltage at 1A/cm^2 and 47% at 5A/cm^2.

As anticipated, the PEMEC temperature affects the I-V curve. When operating at a high temperature, the activation overpotential tends to be reduced, as well as the Gibbs free energy, and the ohmic overpotential. From a thermodynamic point of view, the reaction is more likely to take place at a high temperature, but considering the membrane properties, the temperature is usually kept under the boiling point to avoid dehydration. Temperature also improves the reaction kinetics, increasing the PEMEC efficiency [77] as captured by Eq. (10), Eq. (16), Eq. (13) and Eq. (17).

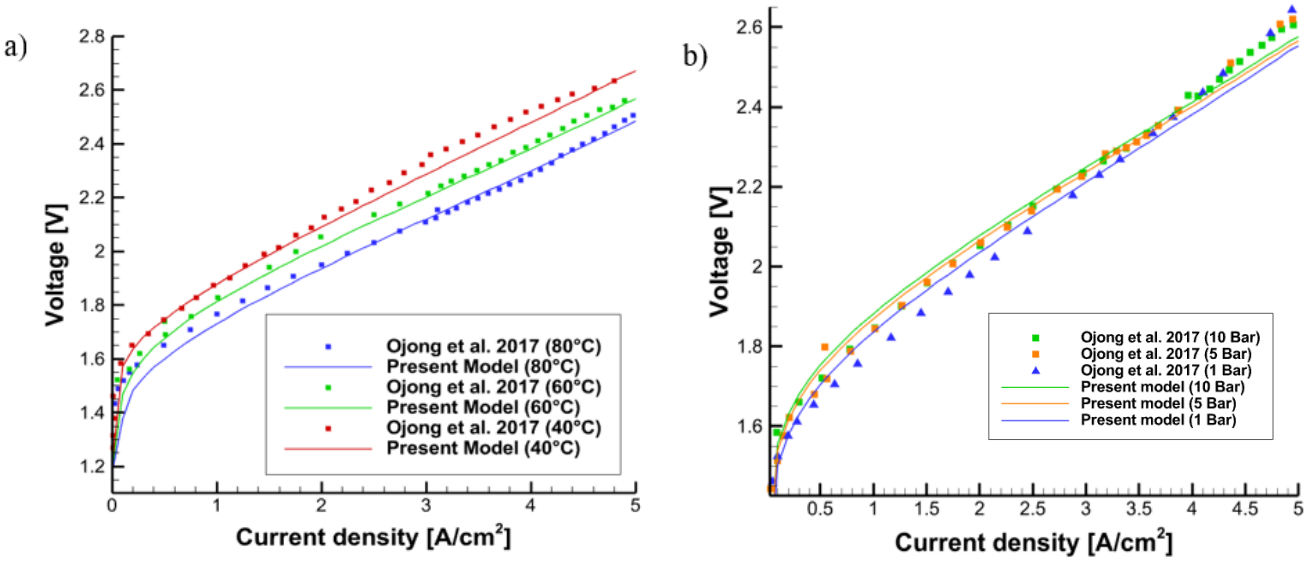

Figure 17. Polarization curve (0-5A/cm^2) comparison at variable a) Temperature and b) Pressure.

Figure 17a presents the effect of temperature on the voltage of the cell (from 40°C to 80°C). The figure shows how the voltage decreases with the increase of temperature, going from ~2.65V at 40°C to ~2.48 at 80°C, thus less energy in form of electricity is needed to complete the

separation water splitting process and the cost of hydrogen production can also be reduced. It is considered that working at higher temperature (under 100℃) is a technique to reach a higher efficiency and a reduction on the price of the hydrogen produced.

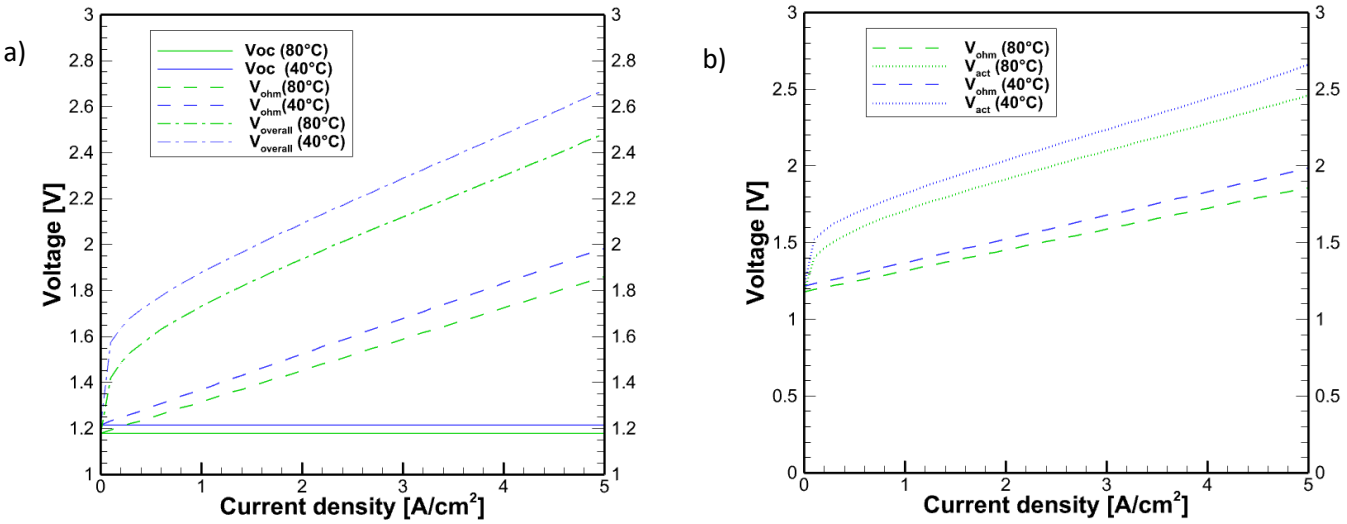

Figure 18. Effects of operating temperature on each overpotential: a) Voc and Vohm and b) Vact.

Figure 18 plots temperature effects on each overpotential, showing that the open-circuit (OC) voltage and ohmic overpotentials are strongly affected by temperature. When working under 40℃ and 5A/cm^2 the open-circuit voltage is ~1.22 V, but when working under 80℃ and at the same current density, this voltage dropped to ~1.18 V. At 40℃ and at the same current density, the ohmic overpotential is ~0.8 V, compared to ~0.68 V at 80℃. Figure 18b makes it possible to see that the activation overpotential increases as temperature decreases. At 80℃ and 5A/cm^2, the activation overpotentials reached ~0.60 V compared to ~0.64 V at 40℃ and 5A/cm^2. Note that in this study, we assume the open-circuit potential is equal to the thermal reversible potential.

Figure 17b reflects the effect of pressure on the PEMEC voltage. It can be inferred that the cell voltage increases as pressure rises, this is because pressure affects the open-circuit voltage of the PEMEC. The small increment with the increase of the operating pressure can be explained by the fact that the other overpotentials remain almost the same. When working at 10 bar, a voltage of ~2.53V and 5 A/cm^2 is achieved, while when working at 1 bar and 5 A/cm^2, a voltage of ~2.48V is reached. Since the increment on pressure shows a very small effect on the cell voltage, it is inferred that working under high pressure results in a lower efficiency since more energy is required to increase the operating pressure, but the losses remain almost the same, hence incrementing the pressure has almost negligible effects on the overall voltage of the PEMEC.

Chapter 4. Conclusions

Hydrogen is a promising energy carrier due to its high-energy density and carbon free feature. It can be obtained from different sources including water electrolysis, being PEM water electrolyzers considered as one of the best solutions for sustainable high purity hydrogen production when coupled with a renewable power source.

In this study, a component-level mathematical model was implemented using MATLAB/Simulink to study the factors affecting PEMECs. The model considered aspects like two-phase transport at the PTL, electrochemical kinetics related to the water splitting reactions, water exchange between the anode and the cathode, proton conductance, two-phase oxygen-liquid in the channel of the cell, and an interfacial sub-model for oxygen removal at the channel/PTL interface. The work aimed to contribute by studying the effects of operating

conditions and mass transport phenomena to each region of the polarization curve. The model assumes 1.) homogeneous properties in each component, 2.) isothermal conditions, and 3.) Tafel equation to approximate electrochemical reaction kinetics.

Using the interfacial sub-model, three different cases of water saturation at the PTL (0.35,0.40, and 0.45) were evaluated to measure their effects in the activation overpotential at the anode side, attributed to the formation of gas bubbles at the anode. The results showed a difference of about 1% between each case. After a comparison with the data available in the literature, a fully liquid water saturation state was assumed until reaching a saturation of 0.45 to be implemented in the model. Once the saturation was selected, the model was tested under different operating conditions, the current densities varied from 0 to **5**A/cm^2**,** temperature from 40℃ to 80℃, the pressure changed from 1 to 10 bar and liquid saturation percentages from 100 to 45%. A porosity of .3, and a PTL and membrane thicknesses of 200µmwere considered.

The simulated results proved to have a good agreement when validated against various experimental data available un the literature. The obtained information shows that ohmic and activation overpotential contribute to a major voltage loss representing about 27% and 19% when working at 5A/cm^2,1 atm, and 80℃. Additionally, when working at high current density, oxygen bubbles are found to occupy an area as large as 55% at the PTL/Ch interface, blocking the available region for water transport to the catalyst layer, reducing the cell performance.

Furthermore, high-temperature operation helps the overall voltage to decrease around 4% when changing from 40℃ to 60℃, and about 8% when changing from 60℃ to 80℃ thanks to the thermal energy added.

The change in operating pressure revealed that the rise in the operating pressure raised the overall voltage of the cell due to its effect on the open-circuit voltage, but this rise is considered small compared to the effects of temperature. From these observations, it can be concluded that operating at relatively high temperature, increases the hydrogen production of the electrolysis cell, and that the material properties should be optimized, as well as the design to improve the gas bubble removal at the channel/PTL interface.

References

1. Abdin, Z., Webb, C. J., & Gray, E. M. (2015). Modelling and simulation of a proton exchange membrane (PEM) electrolyser cell. *International Journal of Hydrogen Energy, 40*(39), 13243-13257.
2. Keçebaş, A., Kayfeci, M., & Bayat, M. (2019). Electrochemical hydrogen generation. In *Solar Hydrogen Production* (pp. 299-317). Academic Press.
3. Arat, H. T., Baltacioglu, M. K., Tanç, B., Sürer, M. G., & Dincer, I. (2020). A perspective on hydrogen energy research, development and innovation activities in Turkey.
4. Awasthi, A., Scott, K., & Basu, S. (2011). Dynamic modeling and simulation of a proton exchange membrane electrolyzer for hydrogen production. *International journal of hydrogen energy*, *36*(22), 14779-14786.
5. Babic, U., Suermann, M., Büchi, F. N., Gubler, L., & Schmidt, T. J. (2017). Critical review—identifying critical gaps for polymer electrolyte water electrolysis development. *Journal of The Electrochemical Society, 164*(4), F387.
6. Bard, A. J., & Faulkner, L. R. (2001). Fundamentals and applications. *Electrochemical Methods, 2*(482), 580-632.
7. Bernt, M., Hartig-Weiß, A., Tovini, M. F., El-Sayed, H. A., Schramm, C., Schröter, J., ... & Gasteiger, H. A. (2020). Current challenges in catalyst development for PEM water electrolyzers. *Chemie Ingenieur Technik, 92*(1-2), 31-39.
8. Bessarabov, D., Wang, H., Li, H., & Zhao, N. (Eds.). (2016). *PEM Electrolysis for Hydrogen Production: Principles and Applications*. CRC press.

9. Briguglio, N., & Antonucci, V. (2016). *Overview of PEM Electrolysis for Hydrogen Production. PEM Electrolysis for Hydrogen Production: Principles and Applications*, 1-9.
10. Busquet, S., Hubert, C. E., Labbé, J., Mayer, D., & Metkemeijer, R. (2004). A new approach to empirical electrical modelling of a fuel cell, an electrolyser or a regenerative fuel cell. *Journal of Power Sources, 134*(1), 41-48.
11. Cai, W., Zhao, X., Liu, C., Xing, W., & Zhang, J. (2014). Electrode Kinetics of Electron-Transfer Reaction and Reactant Transport in Electrolyte Solution. In *Rotating Electrode Methods and Oxygen Reduction Electrocatalysts* (pp. 33-65). Elsevier.
12. Carmo, M., Fritz, D. L., Mergel, J., & Stolten, D. (2013). A comprehensive review on PEM water electrolysis. *International journal of hydrogen energy, 38*(12), 4901-4934.
13. Chen, Q., Wang, Y., Yang, F., & Xu, H. (2020). Two-dimensional multi-physics modeling of porous transport layer in polymer electrolyte membrane electrolyzer for water splitting. *International Journal of Hydrogen Energy, 45*(58), 32984-32994.
14. Chisholm, G., & Cronin, L. (2016). Hydrogen from water electrolysis. In *Storing Energy* (pp. 315-343). Elsevier.
15. Colbertaldo, P., Aláez, S. L. G., & Campanari, S. (2017). Zero-dimensional dynamic modeling of PEM electrolyzers. *Energy Procedia, 142,* 1468-1473.
16. Dale, N. V., Mann, M. D., & Salehfar, H. (2008). Semiempirical model based on thermodynamic principles for determining 6 kW proton exchange membrane electrolyzer stack characteristics. *Journal of Power Sources, 185*(2), 1348-1353.
17. David, M., Ocampo-Martínez, C., & Sánchez-Peña, R. (2019). Advances in alkaline water electrolyzers: A review. *Journal of Energy Storage, 23*, 392-403.

18. Debe, M. K., Hendricks, S. M., Vernstrom, G. D., Meyers, M., Brostrom, M., Stephens, M., ... & Anderson, E. B. (2012). Initial performance and durability of ultra-low loaded NSTF electrodes for PEM electrolyzers. *Journal of the Electrochemical Society, 159*(6), K165.
19. Elia, G. (2015*). Characterization of voltage loss for proton exchange membrane fuel cell* (Bachelor's thesis, Universitat Politècnica de Catalunya).
20. Falcão, D. S., & Pinto, A. M. F. R. (2020). A review on PEM electrolyzer modelling: Guidelines for beginners. *Journal of Cleaner Production, 261*, 121184.
21. Faraj, M., Boccia, M., Miller, H., Martini, F., Borsacchi, S., Geppi, M., & Pucci, A. (2012). New LDPE based anion-exchange membranes for alkaline solid polymeric electrolyte water electrolysis. *International journal of hydrogen energy, 37*(20), 14992-15002.
22. Fritz, D. L., Mergel, J., & Stolten, D. (2014). PEM electrolysis simulation and validation. *Ecs Transactions, 58*(19), 1-9.
23. García-Valverde, R., Espinosa, N., & Urbina, A. (2012). Simple PEM water electrolyser model and experimental validation. *International journal of hydrogen energy, 37*(2), 1927-1938.
24. Godula-Jopek, A. (2015). Hydrogen production: by electrolysis. John Wiley & Sons.
25. Grigoriev, S. A., Millet, P., & Fateev, V. N. (2008). Evaluation of carbon-supported Pt and Pd nanoparticles for the hydrogen evolution reaction in PEM water electrolysers. *Journal of Power Sources, 177*(2), 281-285.
26. Görgün, H. (2006). Dynamic modelling of a proton exchange membrane (PEM) electrolyzer. *International journal of hydrogen energy, 31*(1), 29-38.

27. Han, B., Mo, J., Kang, Z., Yang, G., Barnhill, W., & Zhang, F. Y. (2017). Modeling of two-phase transport in proton exchange membrane electrolyzer cells for hydrogen energy. *International Journal of Hydrogen Energy*, *42*(7), 4478-4489.
28. Hauch, A., Küngas, R., Blennow, P., Hansen, A. B., Hansen, J. B., Mathiesen, B. V., & Mogensen, M. B. (2020). Recent advances in solid oxide cell technology for electrolysis. *Science*, *370*(6513).
29. Ito, H., Maeda, T., Nakano, A., & Takenaka, H. (2011). Properties of Nafion membranes under PEM water electrolysis conditions. *International journal of hydrogen energy*, *36*(17), 10527-10540.
30. IEA (2020). Low-carbon hydrogen production, 2010-2030, historical, announced and in the Sustainable Development Scenario, 2030. Iea.org. Last accessed on 05/11/2021 from: https://www.iea.org/data-and-statistics/charts/low-carbon-hydrogen-production-2010-2030-historical-announced-and-in-the-sustainable-development-scenario-2030
31. IEA (2019), The Future of Hydrogen, IEA, iea.org. Last accessed on 05/11/2021 from: https://www.iea.org/reports/the-future-of-hydrogen
32. Jiang, J. A., Huang, T. L., Hsiao, Y. T., & Chen, C. H. (2005). Maximum power tracking for photovoltaic power systems. Tamkang Journal of Science and Engineering, 8(2), 147.
33. Kalamaras, C. M., & Efstathiou, A. M. (2013). Hydrogen production technologies: current state and future developments. In *Conference papers in energy* (Vol. 2013). Hindawi.
34. Kessler, D. P., & Greenkorn, R. A. (1999). *Momentum, Heat, and Mass Transfer Fundamentals* (No. Sirsi) i9780824719722).

35. Kim, H., Park, M., & Lee, K. S. (2013). One-dimensional dynamic modeling of a high-pressure water electrolysis system for hydrogen production. *International Journal of Hydrogen Energy*, *38*(6), 2596-2609.
36. Kumar, S. S., & Himabindu, V. (2019). Hydrogen production by PEM water electrolysis–A review. Materials Science for Energy Technologies, 2(3), 442-454.
37. Kutscher, C. F., Milford, J. B., & Kreith, F. (2018). *Principles of Sustainable Energy Systems.* CRC Press.
38. Lickert, T., Kiermaier, M. L., Bromberger, K., Ghinaiya, J., Metz, S., Fallisch, A., & Smolinka, T. (2020). On the influence of the anodic porous transport layer on PEM electrolysis performance at high current densities. *International Journal of Hydrogen Energy*, *45*(11), 6047-6058.
39. Liso, V., Savoia, G., Araya, S. S., Cinti, G., & Kær, S. K. (2018). Modelling and Experimental Analysis of a Polymer Electrolyte Membrane Water Electrolysis Cell at Different Operating Temperatures. *Energies*, *11*(12), 3273.
40. Lopata, J., Kang, Z., Young, J., Bender, G., Weidner, J. W., & Shimpalee, S. (2020). Effects of the transport/catalyst layer interface and catalyst loading on mass and charge transport phenomena in polymer electrolyte membrane water electrolysis devices. *Journal of The Electrochemical Society*, *167*(6), 064507.
41. Maggio, G., Nicita, A., & Squadrito, G. (2019). How the hydrogen production from RES could change energy and fuel markets: A review of recent literature. *International Journal of Hydrogen Energy*, *44*(23), 11371-11384.

42. Majasan, J. O., Iacoviello, F., Shearing, P. R., & Brett, D. J. (2018). Effect of microstructure of porous transport layer on performance in polymer electrolyte membrane water electrolyser. *Energy Procedia*, *151*, 111-119.
43. Malkow, T., Pilenga, A., Tsotridis, G., & De Marco, G. (2018). EU Harmonised Polarisation Curve Test Method for Low Temperature Water Electrolysis. *Publications Office of the European Union: Brusselsm, Belgium.*
44. Marangio, F., Santarelli, M., & Cali, M. (2009). Theoretical model and experimental analysis of a high pressure PEM water electrolyser for hydrogen production. International journal of hydrogen energy, 34(3), 1143-1158.
45. Merrill, M. D. (2007). *Water electrolysis at the thermodynamic limit.*
46. Millet, P., Dragoe, D., Grigoriev, S., Fateev, V., & Etievant, C. (2009). GenHyPEM: A research program on PEM water electrolysis supported by the European Commission. *International Journal of Hydrogen Energy*, *34*(11), 4974-4982.
47. Mori, M., Mržljak, T., Drobnič, B., & Sekavčnik, M. (2013). Integral characteristics of hydrogen production in alkaline electrolysers. *Strojniški vestnik-Journal of Mechanical Engineering*, *59*(10), 585-594.
48. Møller, K. T., Jensen, T. R., Akiba, E., & Li, H. W. (2017). Hydrogen-A sustainable energy carrier. *Progress in Natural Science: Materials International*, *27*(1), 34-40.
49. URS, K., Bhat, S. V., & Kamble, V. (2018). On exceeding the solubility limit of Cr+ 3 dopants in SnO2 nanoparticles based dilute magnetic semiconductors. *Journal of Applied Physics*, *123*(16), 161518.
50. Nield, D. A., & Bejan, A. (2006). *Convection in Porous Media* (Vol. 3). New York: springer.

51. Kelly, N. A. (2014). *Hydrogen Production by Water Electrolysis. In Advances in Hydrogen Production, Storage and Distribution* (pp. 159-185). Woodhead Publishing.
52. Newell, R. G., & Raimi, D. (2020). Global Energy Outlook Comparison Methods: 2020 Update.
53. Ni, M., Leung, M. K., & Leung, D. Y. (2006). An electrochemical model of a solid oxide steam electrolyzer for hydrogen production. *Chemical Engineering & Technology: Industrial Chemistry-Plant Equipment-Process Engineering-Biotechnology, 29*(5), 636-642
54. Ni, M., Leung, M. K., & Leung, D. Y. (2008). Energy and exergy analysis of hydrogen production by a proton exchange membrane (PEM) electrolyzer plant. *Energy conversion and management, 49*(10), 2748-2756.
55. Nikitin, A., Milchevskiy, Y., & Lyubartsev, A. (2015). AMBER-II: new combining rules and force field for perfluoroalkanes. *The Journal of Physical Chemistry B, 119*(46), 14563-14573.
56. Oliveira, L. F. L., Jallut, C., & Franco, A. A. (2013). A multiscale physical model of a polymer electrolyte membrane water electrolyzer. *Electrochimica Acta, 110*, 363-374.
57. Olivier, P., Bourasseau, C., & Bouamama, B. (2017). Dynamic and multiphysic PEM electrolysis system modelling: A bond graph approach. *International Journal of Hydrogen Energy*, *42*(22), 14872-14904.
58. Onda, K., Murakami, T., Hikosaka, T., Kobayashi, M., & Ito, K. (2002). Performance analysis of polymer-electrolyte water electrolysis cell at a small-unit test cell and performance prediction of large stacked cell. *Journal of The Electrochemical Society, 149*(8), A1069-A1078.

59. Ojong, E. T., Kwan, J. T. H., Nouri-Khorasani, A., Bonakdarpour, A., Wilkinson, D. P., & Smolinka, T. (2017). Development of an experimentally validated semi-empirical fully coupled performance model of a PEM electrolysis cell with a 3-D structured porous transport layer. *International journal of hydrogen energy*, *42*(41), 25831-25847.
60. Ojong, E. T. (2018). *Characterization of the performance of PEM water electrolysis cells operating with and without flow channels, based on experimentally validated semi-empirical coupled-physics models* (Doctoral dissertation, Brandenburgische Technische Universität Cottbus-Senftenberg).
61. Oyama, S. T., Yamada, M., Sugawara, T., Takagaki, A., & Kikuchi, R. (2011). Review on mechanisms of gas permeation through inorganic membranes. *Journal of the Japan Petroleum Institute*, *54*(5), 298-309.
62. Poullikkas, A., Demokritou, P., Sourkounis, C., & Al-Assaf, Y. (2013). Power Options for the Eastern Mediterranean Region. In Conference Papers in Science (Vol. 2013). Hindawi
63. Peng, L., & Wei, Z. (2020). Energy Conversion from Water to Water: Water Electrolysis and the Hydrogen Fuel Cell. *Engineering*.
64. Rashid, M. M., Al Mesfer, M. K., Naseem, H., & Danish, M. (2015). Hydrogen production by water electrolysis: a review of alkaline water electrolysis, PEM water electrolysis and high temperature water electrolysis. *Int. J. Eng. Adv. Technol*, *4*(3), 2249-8958.
65. RB, H. J. C. C. B. (1954). *Molecular Theory of Gases and Liquids*, John Wiley & Sons

66. Adroher, X. C., & Wang, Y. (2011). Ex situ and modeling study of two-phase flow in a single channel of polymer electrolyte membrane fuel cells. *Journal of Power Sources, 196*(22), 9544-9551.].

67. Ruuskanen, V., Koponen, J., Huoman, K., Kosonen, A., Niemelä, M., & Ahola, J. (2017). PEM water electrolyzer model for a power-hardware-in-loop simulator. *International Journal of Hydrogen Energy*, *42*(16), 10775-10784.

68. Saba, S. M., Müller, M., Robinius, M., & Stolten, D. (2018). The investment costs of electrolysis–A comparison of cost studies from the past 30 years. *International journal of hydrogen energy*, *43*(3), 1209-1223.

69. Santos, D. M., Sequeira, C. A., & Figueiredo, J. L. (2013). Hydrogen production by alkaline water electrolysis. *Química Nova*, *36*(8), 1176-1193.

70. Saebea, D., Patcharavorachot, Y., Hacker, V., Assabumrungrat, S., Arpornwichanop, A., & Authayanun, S. (2017). Analysis of unbalanced pressure PEM electrolyzer for high pressure hydrogen production. *Chemical Engineering Transactions*, *57*, 1615-1620.

71. Seo B, Wang Y. Private communication 2020.

72. Schalenbach, M., Carmo, M., Fritz, D. L., Mergel, J., & Stolten, D. (2013). Pressurized PEM water electrolysis: Efficiency and gas crossover. *International Journal of Hydrogen Energy*, *38*(35), 14921-14933.

73. Spurgeon, J. M., & Lewis, N. S. (2011). Proton exchange membrane electrolysis sustained by water vapor. *Energy & Environmental Science*, *4*(8), 2993-2998.

74. Swiegers, G. F., Terrett, R., Tsekouras, G., Tsuzuki, T., Pace, R., & Stranger, R. (2021). *The Prospects of Developing a Highly Energy-Efficient Water Electrolyser by Eliminating or Mitigating Bubble Effects*. Sustainable Energy & Fuels

75. U.S. Energy Information Administration - EIA - Independent Statistics and Analysis. (2020). Production of hydrogen - U.S. Energy Information Administration (EIA). Eia.gov last accessed 05/11/2021from: https://www.eia.gov/energyexplained/hydrogen/production-of-hydrogen.php

76. Wang, Y., & Chen, K. S. (2011). Effect of spatially-varying GDL properties and land compression on water distribution in PEM fuel cells. *Journal of The Electrochemical Society*, *158*(11), B1292.

77. Wang, Y., & Chen, K. S. (2013). *PEM Fuel Cells: Thermal and Water Management Fundamentals*. Momentum Press.

78. Wang, Y., Diaz, D. F. R., Chen, K. S., Wang, Z., & Adroher, X. C. (2020). Materials, technological status, and fundamentals of PEM fuel cells–a review. *Materials Today*, *32*, 178-203.

79. Wang, Y., Li, W., Ma, L., Li, W., & Liu, X. (2020). Degradation of solid oxide electrolysis cells: Phenomena, mechanisms, and emerging mitigation strategies—A review. *Journal of Materials Science & Technology*, *55*, 35-55.

80. Wang, X., Ramírez-Hinestrosa, S., Dobnikar, J., & Frenkel, D. (2020). The Lennard-Jones potential: when (not) to use it. *Physical Chemistry Chemical Physics*, *22*(19), 10624-10633.

81. Xu, W., & Scott, K. (2010). The effects of ionomer content on PEM water electrolyser membrane electrode assembly performance. International Journal of Hydrogen Energy, 35(21), 12029-12037.

82. Zhang, L., Zhao, H., Wilkinson, D. P., Sun, X., & Zhang, J. (Eds.). (2020). *Electrochemical Water Electrolysis: Fundamentals and Technologies*. CRC Press.

83. Yearbook, G. E. S. (2018). Enerdata 2017. Last accessed on 05/12/2021 from:https://yearbook.enerdata.net/total-energy/world-consumption-statistics.html

84. Yearbook, G. E. S. (2020). Enerdata 2017. Las accesed on 05/12/2021 from: https://yearbook. enerdata. net.

85. Yigit, T., & Selamet, O. F. (2016). Mathematical modeling and dynamic Simulinksimulation of high-pressure PEM electrolyzer system. *International journal of hydrogen energy*, *41*(32), 13901-13914.

86. Yilanci, A. H. M. E. T., Dincer, I., & Ozturk, H. K. (2008). Performance analysis of a PEM fuel cell unit in a solar–hydrogen system. *International Journal of Hydrogen Energy*, *33*(24), 7538-7552.

87. Yodwong, B., Guilbert, D., Phattanasak, M., Kaewmanee, W., Hinaje, M., & Vitale, G. (2020). Proton Exchange Membrane Electrolyzer Modeling for Power Electronics Control: A Short Review. C—*Journal of Carbon Research*, *6*(2), 29.

88. Yodwong, B., Guilbert, D., Phattanasak, M., Kaewmanee, W., Hinaje, M., & Vitale, G. (2020). Faraday's Efficiency Modeling of a Proton Exchange Membrane Electrolyzer Based on Experimental Data. *Energies*, *13*(18), 4792.

89. Zhang, L., Zhao, H., Wilkinson, D. P., Sun, X., & Zhang, J. (Eds.). (2020). *Electrochemical Water Electrolysis: Fundamentals and Technologies*. CRC Press.

90. Zlobinski, M., Schuler, T., Büchi, F. N., Schmidt, T. J., & Boillat, P. (2020). Transient and Steady State Two-Phase Flow in Anodic Porous Transport Layer of Proton Exchange Membrane Water Electrolyzer. *Journal of The Electrochemical Society, 167*(8), 084509.
91. Kélouwani, S., Agbossou, K., & Chahine, R. (2005). Model for energy conversion in renewable energy system with hydrogen storage. *Journal of Power Sources, 140*(2), 392-399.
92. Yao, K. Z., Karan, K., McAuley, K. B., Oosthuizen, P., Peppley, B., & Xie, T. (2004). A review of mathematical models for hydrogen and direct methanol polymer electrolyte membrane fuel cells. *Fuel cells, 4*(1-2), 3-29.
93. Khan, M. J., & Iqbal, M. T. (2005). Dynamic modeling and simulation of a small wind–fuel cell hybrid energy system. *Renewable energy, 30*(3), 421-439.
94. Siegel, C. (2008). Review of computational heat and mass transfer modeling in polymer-electrolyte-membrane (PEM) fuel cells. *Energy, 33*(9), 1331-1352.
95. Han, B., Mo, J., Kang, Z., Yang, G., Barnhill, W., & Zhang, F. Y. (2017). Modeling of two-phase transport in proton exchange membrane electrolyzer cells for hydrogen energy. *International Journal of Hydrogen Energy*, *42*(7), 4478-4489.
96. Sun, X., Simonsen, S. C., Norby, T., & Chatzitakis, A. (2019). Composite membranes for high temperature PEM fuel cells and electrolysers: a critical review. *Membranes*, *9*(7), 83.
97. Wang, Y. (2009). Porous-Media Flow Fields for Polymer Electrolyte Fuel Cells: II. Analysis of Channel Two-Phase Flow. *Journal of the Electrochemical Society, 156*(10), B1134.

98. Mayyas, A., & Mann, M. (2019). Emerging manufacturing technologies for fuel cells and electrolyzers. *Procedia Manufacturing*, *33*, 508-515.

99. Chen, Q., Niu, Z., Li, H., Jiao, K., & Wang, Y. (2021). Recent progress of gas diffusion layer in proton exchange membrane fuel cell: Two-phase flow and material properties. *International Journal of Hydrogen Energy*.

100. Hacker, V., & Mitsushima, S. (Eds.). (2018). *Fuel cells and hydrogen: from fundamentals to applied research*. elsevier.

101. Zhang, J., Wu, J., & Zhang, H. (2013). *PEM Fuel Cell Testing and Diagnosis*. Newnes.

102. Wang, Y., & Feng, X. (2009). Analysis of the reaction rates in the cathode electrode of polymer electrolyte fuel Cells: II. Dual-Layer electrodes. *Journal of The Electrochemical Society*, *156*(3), B403.

103. Wang, Y. (2008). Modeling of two-phase transport in the diffusion media of polymer electrolyte fuel cells. *Journal of Power Sources*, *185*(1), 261-271.

104. Wang, Y., & Chen, K. S. (2011). Elucidating two-phase transport in a polymer electrolyte fuel cell, Part 1: Characterizing flow regimes with a dimensionless group. *Chemical engineering science*, *66*(15), 3557-3567.

105. U.S. Energy Information Administration - EIA - Independent Statistics and Analysis. (2020). Global hydrogen demand by sector in the Sustainable Development Scenario, 2019-2070. Eia.gov last accessed 05/11/2021from: https://www.iea.org/data-and-statistics/charts/global-hydrogen-demand-by-sector-in-the-sustainable-development-scenario-2019-2070

106. Scott, K. (2019). *Introduction to Electrolysis, Electrolysers and Hydrogen Production*.

107. Millet, P., & Grigoriev, S. (2013). *Water electrolysis technologies. Renewable Hydrogen Technologies: Production, Purification, Storage, Applications and Safety*, 19-41.

108. Shayegan, S., Pearson, P. J., & Hart, D. (2009). Hydrogen for buses in London: A scenario analysis of changes over time in refuelling infrastructure costs. *International Journal of Hydrogen Energy*, *34*(19), 8415-8427.

109. Cassir, M., Jones, D., Ringuedé, A., & Lair, V. (2013). Electrochemical devices for energy: fuel cells and electrolytic cells. In *Handbook of Membrane Reactors* (pp. 553-606). Woodhead Publishing.

110. Sheffield, J. W., Martin, K. B., & Folkson, R. (2014). Electricity and hydrogen as energy vectors for transportation vehicles. In *Alternative Fuels and Advanced Vehicle Technologies for Improved Environmental Performance* (pp. 117-137). Woodhead Publishing.